NISTIR 6199

Prediction Based Design of Fire Detection for Buildings with Ceiling Heights Between 9 m and 18 m

William D. Davis and Kathy A. Notarianni
Building and Fire Research Laboratory
Gaithersburg, Maryland 20899

United States Department of Commerce
Technology Administration
National Institute of Standards and Technology

NISTIR 6199

Prediction Based Design of Fire Detection for Buildings with Ceiling Heights Between 9 m and 18 m

William D. Davis & Kathy A. Notarianni
Building and Fire Research Laboratory
National Institute of Standards and Technology
Gaithersburg, Maryland 20899

July 1998

U.S. Department of Commerce
William M. Daley, *Secretary*
Technology Administration
Gary R. Bachula, *Under Secretary for Technology*
National Institute of Standards and Technology
Raymond G. Kammer, *Director*

Prediction Based Design of Fire Detection for Buildings with Ceiling Heights between 9 m and 18 m

William D. Davis and Kathy Notarianni
National Institute of Standards and Technology

1. Introduction

Presently, guidelines for fire detection devices are available for buildings with ceiling heights 9 m or less. The purpose of this paper is to provide the experimental and theoretical background necessary to extend guidelines to ceiling heights between 9 m and 18 m. Based on the results of experiments conducted in 15 m and 22 m high hangars [1], detector activation thresholds and detector spacing are analyzed for both smoke and heat detectors. The hangar experiments included small fires designed to investigate the operation of UV/IR detectors and ceiling mounted smoke detectors as well as large fires which were used to investigate the operation of ceiling mounted heat detectors and sprinklers. Only ceiling mounted detection devices will be analyzed in this paper. The hangar experiments were instrumented and included standard fire detection hardware such as bulb and link operated sprinklers, spot and line-type heat detectors, combination UV/IR detectors, and smoke detectors. Smoke temperature measurements were accomplished using thermocouples.

In addition to the detector threshold study, the predictive capabilities of computer fire model simulations were compared with experimental results [1,2,3]. This comparison, which is based on 12 fire tests, resulted in the development of a new ceiling jet algorithm to model phenomena which had not been included in previous algorithms. The improved algorithm provides a better representation of the development of the ceiling jet temperature to a growing hot layer and a better estimation of plume centerline temperature.

Guidelines are examined, based on the experimental results, for fire detector spacing, placement, and sensitivity. Recommendations concerning the use of computer fire models at these heights are made as a function of fire size and hot layer development. The role of draft curtains will be discussed and their impact on detector activation will be demonstrated.

2. Experiments

Two sites were used to conduct the hangar experiments. The first site was a warm temperature site ($\approx$ 30 °C) at Barbers Point, Hawaii and the second site was a cool temperature site ($\approx$ 12 °C) at Keflavik, Iceland. At the Barbers Point site, a total of thirteen fire experiments were conducted (see table 1). Six of the experiments included a draft curtain 3.7 m deep which enclosed an area of dimensions 18.3 m x 24.4 m. The hangar measured 97.8 m x 73.8 m in area and had a ceiling height at the center of 15.1 m. The ceiling height at the center of the draft

curtained area was 14.9 m. As an aid in describing the experimental set up, the directions east and west will be used to describe directions pointing parallel to the 24.4 m side of the draft curtain while north and south will be used to describe directions perpendicular to the 24.4 m side. A plan view of the hangar bay is shown in figure 1.

Table 1 Test summary for 15 m facility. Activation times (Act.) represent the first time that a detector activated at that distance from plume center. S.P. denotes a single point smoke detector located 3.1 m from plume center. P.B. denotes a projected beam detector with the beam located 0.3 m beneath the ceiling and passing through plume center. T in the smoke detector column stands for a trouble signal. The sprinklers (QR for quick response) were located 3.1 m from plume center. The test numbers with an "*" did not have a draft curtain and "**" is an open door test. The term n/a stands for not available. Additional detail is available in reference 1.

Test #	Pan/Crib Size m	Fire Size (1 ± 10%) MW	Fuel Type	Sprinkler Act. s (Wet Pipe) (QR 79°C)	Smoke Det. Act. s (P.B./ S.P.) ± 10. s
1	0.3 x 0.3	0.1	JP - 5	No	75/382.
2	0.6 x 0.6	0.5	JP - 5	No	T/28
3	0.9 x 0.9	1.1	JP - 5	No	T/37
4	1.5 Dia.	3.1	JP - 5	No	T/22
5	2.0 Dia.	6.8	JP - 5	192 ± 10	T/29
6	2.5 Dia.	7.7	JP - 5	104 ± 10	T/28
7*	2.0 Dia.	5.6	JP - 5	403 ± 10	T/26
8*	2.5 Dia.	7.7	JP - 5	359 ± 10	T/26
9*	0.6 x 0.6 x 0.6	0.4	Wood Crib Fir	No	66/52
10*	0.6 x 0.6 x 1.2	0.6	Wood Crib Fir	No	67/58
11*	0.3 x 0.3	0.1	JP - 5	No	73/504
12*	0.6 x 0.6	n/a	JP - 5	No	T/50
13**	2.0 Dia.	n/a	JP - 5	No	T/38

The hangar roof consists of built-up tar and gravel over a corrugated metal deck. The ceiling slopes from a height of 15.1 m at the center toward the east and west walls which are 13.4 m high. The metal deck is directly supported by 0.25 m I beams which run the (N-S) width of the hangar and are spaced 4.1 m on center. The I beams are supported by open steel trusses which run perpendicular to the beams (E-W) and are spaced 6.1 m on center. These trusses span the full length of the hangar.

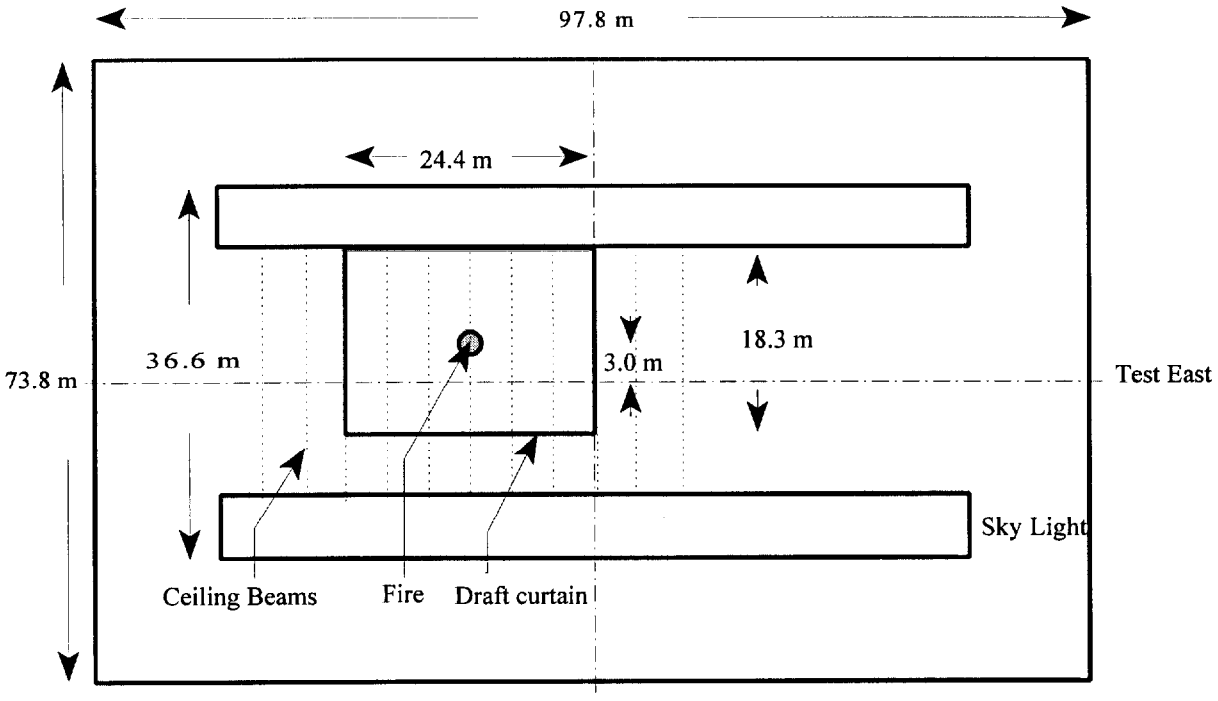

Figure 1 Plan view of 15 m hangar bay.

Thermocouples were used to measure the ceiling jet temperature at radial distances from plume center of 1.5 m, 3.0 m, 6.1 m, 9.1 m, and 11.6 m in the experimental east and west directions, and at 1.5 m, 3.0 m, 6.1 m, and 8.5 m in the experimental north and south directions.

The thermocouples were located 0.31 m beneath the ceiling. The r/H value (r is the radial distance from the plume center and H is the height of the ceiling above the fire surface) for the 1.5 m thermocouples is 0.1 which means that these thermocouples are in the plume. All the

other thermocouples were located outside the plume region. Four thermocouple trees with thermocouples located at 0.15 m, 0.3 m, 0.46 m, 0.61 m, and 0.76 m beneath the ceiling were located 6.1 m from plume center in the north, south, east, and west directions, while a fifth tree with thermocouples located at 0.15 m, 0.3 m, 0.46 m, 0.76 m, 1.22 m, and 3.0 m beneath the ceiling was located at 9.1 m toward experimental east. These thermocouple trees are used to investigate the temperature dependence of the ceiling jet as a function of distance beneath the ceiling.

In the 15 m high facility, nine types of standard spray, upright sprinklers with several different temperature ratings, fusible elements, and response time indexes were installed and monitored to measure the activation time of each sprinkler head when subject to a range of experimental fires. The pipe supplying the sprinkler heads was filled with water to simulate the heat sink associated with a wet-pipe sprinkler configuration. The water was not pressurized and hence only a negligible amount of water would be released when the sprinkler activated. In addition, several sections of piping were used within the individual sprinkler trees to simulate a dry-pipe or pre-action sprinkler system. The sprinkler types and locations with respect to the fire plume are given in table 2. The sprinkler deflectors were installed approximately 300 mm to 360 mm below the ceiling deck.

Photoelectric smoke detectors and electronic heat detectors were connected to an addressable fire alarm control panel via signaling line circuits wired in the Style 4 configuration [4]. The photoelectric smoke detectors were analog addressable spot type detectors which operate according to the light scattering principle. These detectors contain a pulsed LED and silicon photodiode receiver arranged so that light does not fall on the receiver. When smoke particles enter the light path, light strikes the particles and is scattered onto the photosensitive receiver, causing the detector to respond. The smoke detector sensitivity threshold was 8.2 % per meter of smoke obscuration.

Table 2 Sprinkler locations (x) measured radially from the plume centerline for the 15 m hangar. All sprinklers have bulbs except for the column marked Link. Distances are given for both the E-W and N-S directions. Due to the rectangular shape of the draft curtain (24.4 m x 18.3 m) the 11.6 m location in the N-S direction was outside the draft curtain (OD). The sprinklers are listed by activation temperature and response time index (QR = 35 $(ms)^{1/2}$, STD = 188 $(ms)^{1/2}$, and Link = 95 $(ms)^{1/2}$). All sprinklers were connected to water filled pipes except for those sprinklers labeled "dry" which were connected to empty pipes.

Distance m E-W/N-S	79 °C QR	79 °C QR dry	79 °C STD	93 °C QR	141 °C QR	141 °C QR dry	141 °C STD	141 °C Link	182 °C STD
0.0	x	x	x	x	x	x	x	x	x
3.0/3.0	x	x			x	x	x	x	
6.1/6.1	x				x		x	x	
9.1/8.5	x				x				
11.6/OD	x				x				

The electronic heat detectors were analog addressable spot type detectors which were programmed to operate as fixed temperature heat detectors with an alarm threshold of 57.2 °C. This type of detector employs a non-metallic thermistor and experiences little thermal lag in its response to changing temperatures.

There were 18 detector stations each consisting of a smoke detector and a heat detector mounted to a plywood board. The plywood board was suspended from conduit which was clamped to the underside of the I beams supporting the metal roof deck. Given that the ratio of the beam depth to ceiling height was less than 0.1, and that the ratio of the beam spacing to the ceiling height was less than 0.4, the detectors were installed at the same elevation as the bottom of the beams which was 0.25 m below the ceiling deck. The detector stations within the draft curtained area were located at distances from plume center of 3.0 m, 6.1 m, 9.1 m, and 11.6 m in the E-W direction and 3.0 m, 6.1 m, and 8.5 m in the N-S direction.

Projected beam smoke detection systems are photoelectric smoke detectors that consist of separate transmitters and receivers. The light source in the transmitter produces an infrared beam that is measured by the receiver to determine obscuration caused by smoke. If the beam intensity falls below an alarm threshold and remains there for a preset length of time, a fire alarm is initiated. If complete beam blockage occurs, a trouble output is generated rather than a fire

alarm. The receiver will wait a preset length of time after the beam is blocked before giving a trouble signal. Gradual loss of signal due to dust/dirt build-up and other long-term effects is automatically compensated for by the receiver up to a point where the signal has been reduced by 50 %. When 50 % of the signal is lost, the receiver will give a trouble signal [5].

The projected beam smoke detectors were configured to view paths through plume center and 7.0 m on either side of plume center for distances beneath the ceiling of 0.3 m, 2.7 m, and 5.8 m for tests 1 through 8. The beam lengths were 24.4 m with the beams directed perpendicular to the 0.25 m deep ceiling I beams. Tests 1 through 6 had a 3.7 m deep draft curtain in place which meant that the 5.8 m paths were substantially below the bottom of the draft curtain. Tests 9 through 13 substituted the 5.8 m paths with a single path located 1.8 m beneath the ceiling and passing through plume center.

Table 3 Test summary for fire sizes smaller than 3 MW for the 22 m facility. Activation times represent the first time that a detector activated at that distance from the fire. S.P. denotes a single point smoke detector which was located 3.1 m from plume center. P.B. denotes a projected beam detector with the beam located 1.3 m beneath the ceiling and passing through plume center. The sprinklers were located 3.1 m from plume center.

Test #	Pan Size m	Fire Size (1 ± 10%) MW	Fuel Type	Sprinkler Act. s (Wet Pipe) (QR 79 °C)	Smoke Det. Act. s (P.B./S.P.) ± 10 s
1	0.3 x 0.3	0.1	JP - 5	No	53/No
2	0.3 x 0.3	0.1	JP - 5	No	60/No
3	0.6 x 0.6	0.9	JP - 5	No	36/53
4	0.6 x 0.6	0.8	JP - 5	No	19/51
5	0.9 x 0.9	1.7	JP - 5	No	25/28
6	0.9 x 0.9	1.4	JP - 5	No	31/32
7	1.2 x 1.2	2.8	JP - 5	No	31/36
8	1.2 x 1.2	2.5	JP - 5	No	27/33
9	0.3 x 0.3	0.1	JP - 8	No	108/No
10	0.6 x 0.6	0.6	JP - 8	No	47/150
11	0.6 x 0.6	0.8	JP - 8	No	35/90
12	0.9 x 0.9	1.6	JP - 8	No	34/45
13	1.2 x 1.2	2.7	JP - 8	No	37/37

A total of 21 pan fire experiments were conducted at Keflavik, Iceland (see table 3 for tests with HRR less than 3 MW and table 4 for tests with HRR greater than 3 MW). The Keflavik hangar measured 73.8 m by 45.7 m and had a barrel roof which was 22.3 m high at the center and 12.2 m high at the walls. Corrugated steel draft curtains were used to divide the ceiling into five equal bays approximately 14.8 m by 45.7 m with the fire experiments conducted in the middle bay and centered under the 22.3 m high ceiling.

Table 4 Test summary for fire sizes larger than 3 MW for the 22 m facility. Activation times represent the first time that a detector activated at that distance from the fire. Activation times for detectors should include a ± 10 s uncertainty in establishing the start time of the experiment. P.B. denotes a projected beam smoke detector with the beam located 1.3 m below the ceiling and passing through plume center and S.P. denotes a single point smoke detector located 3.1 m from plume center. The sprinklers were located 3.1 m from plume center. T in the smoke detector column stands for a trouble signal. The test numbers with an "**" were open door tests.

Test #	Pan Size m	Fire Size (1 ± 10%) MW	Fuel Type	Sprinkler Act. s (Wet Pipe) (QR 79 °C)	Smoke Det. Act. s (P.B./S.P.) ± 10 s
14	2.5	7.9	JP - 5	361.± 10.	38/65.
15	3.0 x 3.0	15.7	JP - 5	119.±10.	33/46.
16**	2.5	7.0	JP - 5	No	T/51.
17	3.0 x 3.0	14.3	JP - 8	100.±10.	27/30.
18	2.0	4.9	JP - 5	No	42/49.
19**	2.5	9.1	JP - 5	No	39/56.
20	3.0 x 3.0	14.6	JP - 5	101.±10.	31/38.
21	4.6 x 4.6	33	JP - 5	87.±10.	30/37.

The primary roof support consisted of a series of steel trusses which form arches spanning the

width of the hangar bay, running parallel to the hangar doors. These primary trusses are approximately 1.0 m deep and are spaced 7.4 m on center. The primary trusses are interconnected with a series of secondary trusses which are perpendicular to them and run the length of the hangar bay. The secondary trusses are spaced at intervals ranging from 5.8 m to 6.4 m on center. The metal deck roof is directly attached to a series of steel beams which sit on top of the primary and secondary trusses. These steel beams are perpendicular to the primary trusses, are spaced 1.5 m to 2.1 m on center, and vary in height from 0.2 m to 0.3 m.

The roof was insulated via a barrel shaped suspended tile ceiling which was supported by a conventional suspended tile ceiling grid located at the same elevation as the bottom of the steel beams. The individual ceiling tiles in the center bay and the adjacent bay were removed prior to testing.

Experimental east and west were designated to be the directions parallel to the 13.4 m draft curtain and pointed along the direction of the barrel roof. Experimental north and south directions ran perpendicular to the draft curtain. Thermocouples located 0.31 m beneath the ceiling were at radial distances from fire center of 3.0 m, 4.6 m, 6.1 m, and 6.7 m in the south direction and 3.0 m and 6.1 m in the north direction. Thermocouples located 0.31 m beneath the ceiling were at radial distances from fire center of 3.0 m, 6.1 m, 9.1 m, 12.2 m, 15.2 m, and 18.3 m. Additional thermocouples were positioned at many of these locations and are represented in figure 2.

The same kinds of sprinklers, spot heat and smoke detectors, and beam smoke detectors that were used in the 15 m hangar tests were used in the 22 m tests. In addition, conventional hard-wired heat detectors using a thermistor-type sensing element with an alarm threshold of 93.3 °C were included. The eighteen detector stations consisted of a smoke detector and the two types of heat detectors (57 °C and 93 °C). These detector stations were located at distances of 3.0 m and 6.1 m from plume center in the north and south directions and 3.0 m, 6.1 m, 9.1 m, 12.2 m, 15.2 m, and 18.3 m from plume center in the east and west directions along the curved ceiling. The detector stations were located at approximately the same elevation as the sprinklers which ranged from 0.3 m to 0.6 m below the ceiling deck. The sprinkler locations with respect to plume center are given in table 5. Additional details concerning the installation of these detectors are available in reference 1.

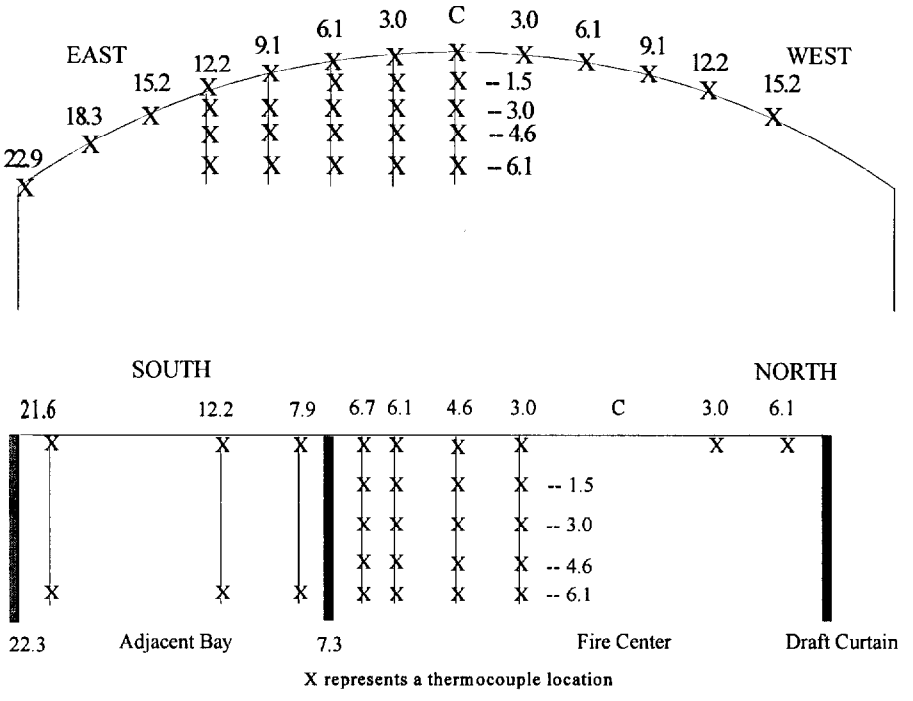

Figure 2 Thermocouple locations (in m) for the hangar at Keflavik

Table 5 Sprinkler locations (x) measured radially from the plume centerline for the 22 m hangar. The distances marked OD in the N-S direction represent locations outside the draft curtained area. The sprinklers are listed by activation temperature and response time index (QR = 35 $(ms)^{1/2}$, STD = 188 $(ms)^{1/2}$, and STD Link = 95 $(ms)^{1/2}$). All sprinklers were connected to water filled pipes except for those sprinklers labeled "dry" which were connected to empty pipes.

Distance m E-W/N-S	79 °C QR	79 °C QR dry	79 °C STD	93 °C QR	141 °C QR	141 °C QR dry	141 °C STD	141 °C STD Link	182 °C STD
0.	x	x	x	x	x	x	x	x	x
3.0/3.0	x	x			x	x	x	x	
6.1/6.1	x				x		x	x	
9.1/OD	x				x				
12.2/OD	x				x				
15.2/OD	x				x				

3. Modeling Algorithms

3.1 Plume Centerline Temperature

The observed characteristics of the fire plume and ceiling jet in these experiments can best be characterized in terms of existing fire correlations and fire models. Several correlations exist for the calculation of plume centerline temperature. Perhaps the most widely used correlation is one developed by Heskestad [6] which gives the centerline excess temperature ΔT as a function of height above a virtual point source to be

$$\Delta T = 9.1\left(\frac{T_\infty}{g c_p^2 \rho_\infty^2}\right)^{1/3} Q_c^{2/3} (z - z_0)^{-5/3} \qquad \textbf{(1)}$$

The virtual origin is given by

$$z_o = -1.02D + 0.083Q^{2/5} \tag{2}$$

where Q and Q_c are the total and the convective heat release rates, D is the pool diameter, z is the height above the fire surface, and T_∞, c_p, and ρ_∞ are the temperature, heat capacity, and density of the ambient gas. This correlation was developed for unconfined ceilings where an upper layer does not form.

When an upper layer forms, this correlation must be modified in order to correctly predict plume centerline temperature since the plume now includes added enthalpy by entraining hot layer gas as it moves through the upper layer to the ceiling. Methods involving defining a substitute virtual source applicable to the upper layer have been developed by Cooper [7] and Evans [8]. Evans' method defines the strength Q_I^* and location Z_I of the substitute source by

$$Q_{I,2}^* = [(1 + C_T Q_{I,1}^{*2/3})/\xi C_T - 1/C_t]^{3/2} \tag{3}$$

and

$$Z_{I,2} = [\frac{\xi Q_{I,1}^* C_T}{Q_{I,2}^{*1/3}[(\xi - 1)(\beta^2 + 1) + \xi C_T Q_{I,2}^{*2/3}]}]^{2/5} Z_{I,1} \tag{4}$$

where I refers to the layer interface, 1 and 2 refer to the lower and upper layer, ξ is the ratio of upper to lower layer temperature, β is the velocity to temperature ratio of Gaussian profile half widths, and $C_T = 9.115$. The new ceiling height is then obtained from

$$H_2 = H_1 - Z_{I,1} + Z_{I,2} \tag{5}$$

where $Z_{I,1}$ is the height from the fire to the layer interface and H_1 is the location of the fire beneath the ceiling. The new values of the fire source and ceiling height are then used in the standard plume correlations where the ambient temperature is now the temperature of the upper layer.

Early in a high bay fire, prior to the development of the ceiling layer, the plume centerline

temperature should follow Heskestad's unconfined ceiling correlation. As the ceiling layer develops, the impact of the layer on plume centerline temperature should increase as hot layer gases are entrained into the plume. Zone fire models available at NIST include CFAST [9], FPEtool [10], and LAVENT [11]. Of these models, only the Fire Simulator part of FPEtool presently contains a plume centerline temperature algorithm which incorporates the impact of the upper layer on the temperature. FPEtool makes use of Evans' method to calculate a substitute source and location for the upper layer. It then makes use of a ceiling jet correlation developed by Alpert [12] to calculate the plume centerline temperature. Alpert's correlation assumes that the plume temperature remains a constant for distances less than $r/H = 0.18$ where r is the distance from plume center and H is the distance between the fire and the ceiling.

Since the temperature in the plume is observed to increase toward plume center, the assumption of constant temperature throughout should underpredict the centerline temperature. A new zone fire model, JET, was developed to test this observation. In this model, the method of Evans was used to account for the entrained enthalpy from the upper layer while the correlation of Heskestad and Delicahtsios [13] was used to obtain the plume centerline temperature as suggested in Evans' paper. The algorithms used for the layer depth and temperature calculations were taken from LAVENT after modification to include a user determined radiative fraction.

Figure 3 shows the plume centerline temperature at approximately 200 s for eleven experiments which developed upper layers. The first two experiments were conducted at Barbers Point and carry a "B" designator, while the remainder were conducted at Keflavik. All experiments used JP-5 except the one designated "8" in Keflavik which used JP-8. The total heat release rate is shown for each experiment. Also shown in the figure are the predictions of the plume correlation of Heskestad (Hesk), the plume model of Evans as calculated in version 3.2 of FPEtool (FPEtool), and the prediction of the Evans' model in JET (JET).

The following assumptions were used for all model calculations. Only the draft curtained area was modeled. This modeling assumption was reasonable early in the tests since both buildings were large enough that it required in excess of 200 s for the entire ceiling to fill with smoke down to the bottom of the draft curtains. The steady state heat release rate was used in each of the

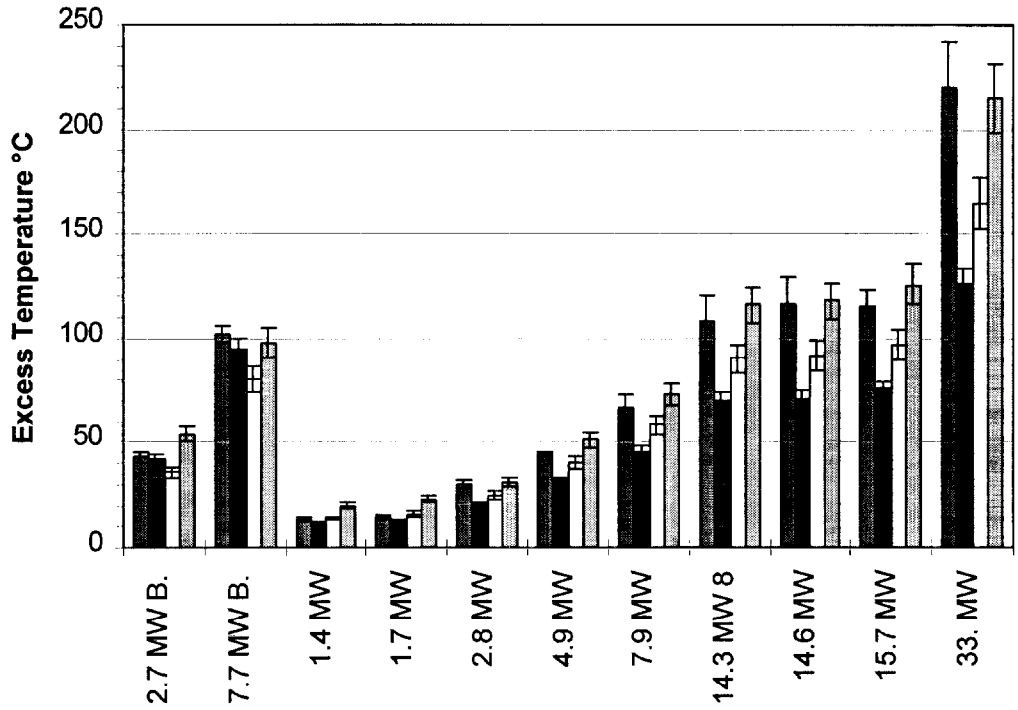

Figure 3 Comparison of measured plume centerline temperature at 200 s after ignition, the first column from the left in each group, with plume centerline calculations using Heskestad's algorithm, FPEtool, and JET in the second through fourth columns respectively. Two of the eleven experiments were conducted in the 15 m hangar and are labeled "B" while the others were in the 22 m hangar. The experiments are designated according to their steady-state total heat release rate. All fires were JP-5 pan fires with the exception of the 14.3 MW fire which was a JP-8 pan fire and is labeled with an "8" on the figure.

calculations. The radiative fraction was calculated using the correlation

$$\chi_r = 0.35 * (2.0/D)^{0.6} \qquad (6)$$

where χ_r is the radiative fraction and D is the fire diameter. This correlation for radiative fraction was developed for kerosene [14] but should apply for JP-5 and JP-8 owing to their similar chemical makeup. The correlation is valid for pan diameters in excess of 1.0 m.

The uncertainty intervals shown on the data in figure 3 are one sigma intervals deduced from

doing a least squares time average of five data points taken over a 20 s measurement period for the centerline thermocouple located 0.3 m below the ceiling. These intervals represent the scatter in the measurements which come from a combination of plume sway and fire puffing. A small amount of electronic noise is also included in the intervals.

No radiation corrections were made to the thermocouple measurements since the smoke surrounding the thermocouples made the environment optically thick. While the absolute uncertainty in thermocouple measurements as reported by the manufacturer is ±2 °C, at the start of each experiment, the thermocouples used in the analysis registered the same ambient temperature to within 1 °C.

Three of the fire tests conducted at Keflavik were 3.0 m square pan fires, two JP-5 and one JP-8 . These three tests provided an indication of repeatability for the experiments in that the average heat release rate for the three tests were (14.8 ± 0.7) MW. While JP-8 has a lower flash point than JP-5, the cone calorimeter tests for the two fuels indicated that their heat release rates were identical within the relatively uncertainty of the cone calorimeter [1]. Therefore, the JP-8 test was included with the JP-5 tests to examine repeatability.

Measurements that were used in the fire model calculations that would most affect their predictions include the heat release rate and the radiative fraction as a function of pan diameter. The accuracy of the total heat release rate depends on the accuracy of the load cell and of the heat of combustion of the fuel. Relative uncertainties in the heat release rate were estimated to range from 5% to 10% for the fire tests used in this paper. Adding an estimated relative uncertainty of 5% for the uncertainty in radiative fraction, the relative uncertainty in the convective heat release rate should be 15%. A relative uncertainty of 15% in the convective heat release rate would yield a relative uncertainty of 10% to 15% in the temperature predictions of the correlations and computer models used in this paper.

The 10% relative uncertainty applies to the models with no layer interaction since the excess temperature scales as the convective heat release rate to the 2/3 power. For the models which include a layer interaction, sensitivity studies indicate approximately a 10% to 15% relative uncertainty in the temperature calculation for a relative uncertainty of 15% in the convective heat release rate. The uncertainty intervals shown in figure 3 for the model calculations represent a ± 5% relative uncertainty for Heskestad's plume theory and ± 7.5% relative uncertainty for the two computer model calculations.

The correlation and computer models performed as expected. The correlation of Heskestad underpredicted the plume centerline temperature for most of the experiments with the largest differences occurring for the largest fires which produce the hottest layers. The computer model FPEtool also underpredicted the plume centerline temperatures as expected based on the algorithms used in the model. The computer model JET provided excellent predictions for the large fires but did overpredict the plume centerline temperature of the smallest fires. This overprediction of small fires could result from the sensitivity of the calculations to the layer temperature when the layer temperature is close to ambient.

3.2 Ceiling Jet Temperature Radial Variation

The flow of hot plume gas along the ceiling directed radially away from the fire plume is defined as the ceiling jet. The ceiling jet may be represented by temperature and velocity distributions which vary both radially away from the fire center and vertically below the ceiling. The development of a ceiling jet model is complicated by the fact that in an enclosure, a hot gas layer forms near the ceiling which interacts with the ceiling jet.

One of the earliest ceiling jet models was developed by Alpert [12]. This model was based on the ceiling jet flow produced by steady fires for an unconfined ceiling, a ceiling where a gas layer will not form. For $r/H \geq 0.18$, the ceiling jet excess temperature falls off as $r^{-2/3}$. The temperature is assumed to remain at the value obtained for $r/H = 0.18$ for $r/H < 0.18$. This particular correlation is available in the computer programs DETACT-QS [15] and FPEtool [10]. A second steady state ceiling jet correlation developed by Heskestad and Delichatsios [13] gives the excess temperature as

$$\Delta T = T_\infty (Q^*)^{2/3} / (0.188 + 0.313 r/H)^{4/3} \tag{7}$$

$$Q^* = Q / (\rho_\infty C_p T_\infty g^{1/2} H^{5/2}) \tag{8}$$

When the ceiling jet is confined and a hot layer forms, the presence of the layer must be included in the calculations. Methods of treating the ceiling jet in the presence of a hot layer have been developed by Evans [8] and Cooper [7]. A modified version of Evans' method is presently used in the computer fire model FPEtool while Cooper's method is used in the fire models LAVENT [11] and CFAST [9]. Evans' method uses the strength and location of the substitute source as calculated in equations 3 - 5 which are then substituted in the ceiling jet correlation of Heskestad and Delichatsios. In FPEtool, the ceiling jet correlation of Alpert rather than Heskestad and Delichatsios is used. The layer temperature and layer height needed in the calculations are supplied by a single room zone model in FPEtool.

Cooper's method includes additional phenomena such as modeling the ceiling jet temperature as a function of depth beneath the ceiling and including the possibility that some of the entrained air does not have sufficient buoyancy to enter the upper layer. Also included in the algorithm is a radially dependent heat loss calculation to the ceiling. The zone models LAVENT and CFAST use different plume algorithms to calculate the response of the upper layer to the fire; hence the results obtained using this algorithm in the two models may yield somewhat different results.

These models account for the interaction of the plume with the layer resulting in a hotter plume

at the ceiling. The models may not account for the presence of the hot gas layer impacting the energy loss of the ceiling jet. The hot gas layer should reduce the radiation loss from the ceiling jet and eliminate the mixing of cool gas into the ceiling jet. The end result should be that the temperature decrease with radial distance should lessen as the ceiling jet becomes more adiabatic. This effect has been observed in hood experiments [16].

While the hood experiments were steady state experiments, the high bay experiments allow the ceiling jet temperature dependence to be followed in time. An excellent example of the evolution of the radial temperature dependence of the ceiling jet in time is displayed by the 2.8 MW JP-5 pan fire with draft curtain at Keflavik (Fig. 4). The experimental values are based on an average of five data points over a 20 s interval centered on the given time with the typical one sigma uncertainty shown on only one of the curves to avoid cluttering the figure. Figure 4 shows

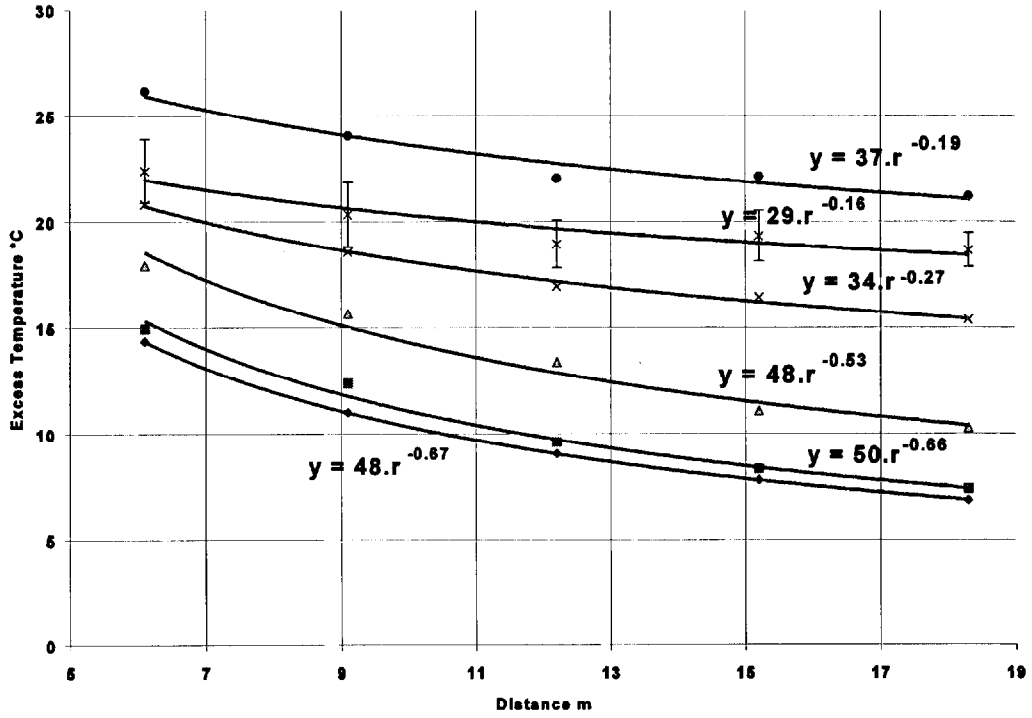

Figure 4 Time evolution of the radial temperature dependence of the ceiling jet for the 2.8 MW JP-5 pan fire at Keflavik. The measurements are averaged on the east and west sides of plume center in the direction of the barrel roof. The lowest curve is Alpert's correlation with the next five curves representing the experiment at times of 80 s, 100 s, 150 s, 200 s, and 300 s. Power law curve fits are given for each data set and Alpert's correlation as a function of distance, r, from plume center.

the temperature evolution in time as well as a comparison to Alpert's ceiling jet correlation. Early in time before a hot layer forms, the temperature dependence of the ceiling jet mirrors Alpert's correlation. The measurements were made in the east direction which is in the direction of the barrel roof. The sloping roof appears not to have produced a significant impact on the

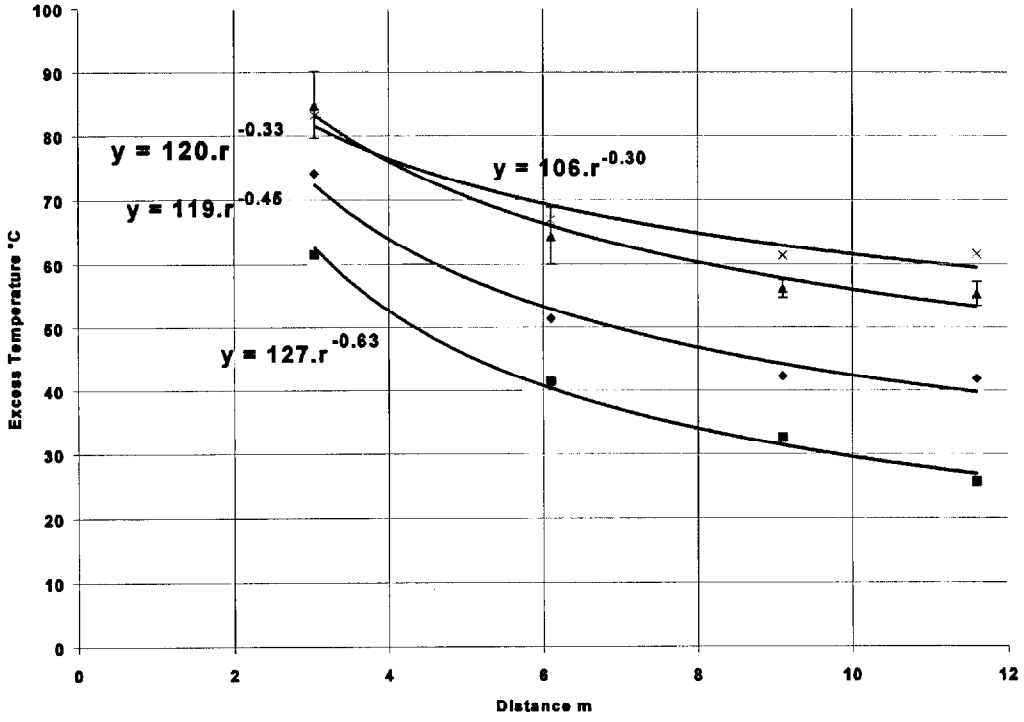

Figure 5 7.7 MW JP-5 pan fire with draft curtain at Barber's Point. The four curves correspond to experimental times of 70 s, 100 s, 200 s, and 300 s from bottom to top respectively.

ceiling jet temperature until the distance from plume center exceeded 20 m. As the layer formed, the radial dependence of the temperature decreased significantly as the overall temperature of the jet increased due to the entrainment of the hot layer by the plume. This evolution of ceiling jet temperature is evident in all data sets.

Another excellent example would be the 7.7 MW JP-5 pan fire with draft curtain at Barbers Point as shown in figure 5. This ceiling had a negligible slope. Early in time, Alpert's correlation ($r^{-0.67}$) would provide a reasonable fit to the radial temperature dependence of the ceiling jet. At later times, the temperature dependence shows a diminished dependence on radial distance from plume center and an increasing overall temperature as the layer depth increases.

As a final example of the time evolution of the ceiling jet, the ceiling jet excess temperatures for the 4.9 MW, 7.9 MW, 14.6 MW and 15.7 MW JP-5 pan fire tests at Keflavik were scaled to the ceiling jet excèss temperature of the 2.8 MW test using the 2/3 power of the convective heat release rate for each experiment. The scaled excess temperatures were averaged with the results presented in figure 6 for an early time before a layer could form and at 200 s when the layer should fill the draft curtained area. The power law fit for the no layer situation ($r^{-0.73}$) is indistinguishable from the Alpert correlation ($r^{-0.67}$). At later times, the radial dependence of the ceiling jet temperature flattens markedly as the overall temperature of the ceiling jet increases due to the impact of the layer. The uncertainty intervals shown on the figure represent the one sigma interval deduced from averaging the scaled temperatures at each point from the five tests.

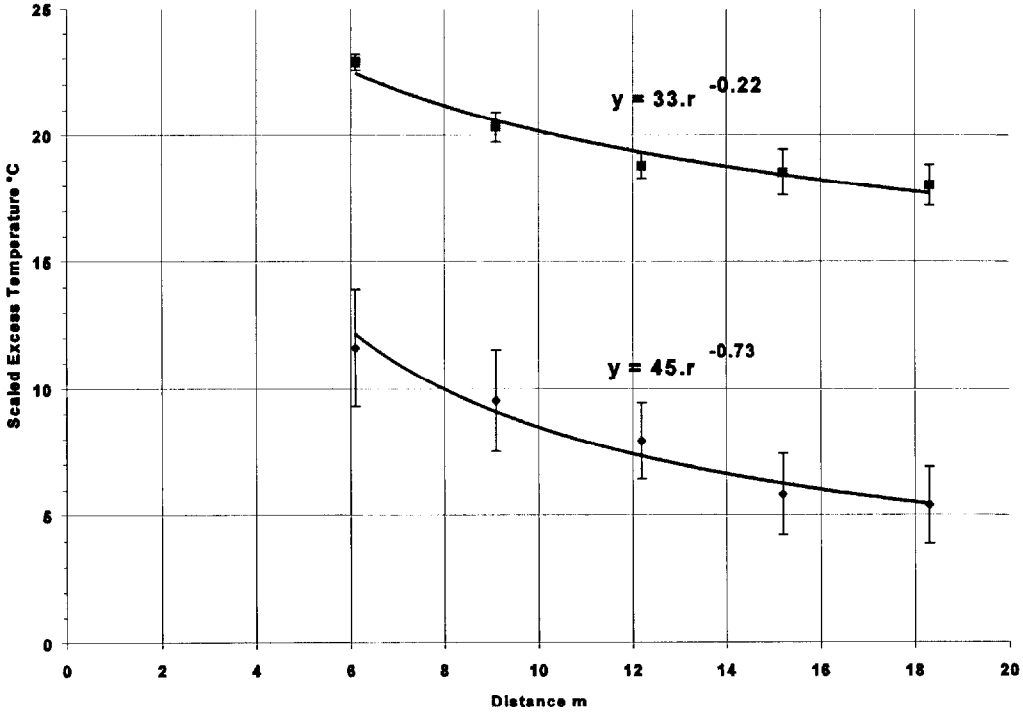

Figure 6 Averaged ceiling jet temperature for the 2.8 MW, 4.9 MW, 7.9 MW, 14.6 MW and 15.7 MW tests at Keflavik. The bottom curve represents the ceiling jet with no layer while the top curve represents the ceiling jet at 200 s after a layer has filled the draft curtains. Temperatures are scaled to the convective heat release rate of the 2.8 MW test.

In order to include the observed changes in both the magnitude and radial dependence of the temperature in the ceiling jet, the following modification to Alpert's correlation is proposed. The ceiling jet temperature excess ΔT as a function of radius for $r/H > 0.18$ is given by

$$\Delta T = C/r^{\gamma} \tag{9}$$

$$C = \beta r_o^{\gamma} \Delta T_p \tag{10}$$

where

$$\beta = (0.68 + 0.16(1 - e^{-y_L/y_J})) \tag{11}$$

$$r_o = 0.18H \tag{12}$$

$$\gamma = 2/3 - \alpha(1 - e^{y_L/y_J}) \tag{13}$$

and $\alpha = 0.44$, $y_j = 1.0$ m, y_L is the layer thickness, and ΔT_p is the plume centerline temperature excess as calculated using Evans' method (equations 3-5 & 7-8). The value of α is determined by the requirement that with no hot layer, the radial dependence on the ceiling jet temperature should follow Alpert's value of 2/3, while after the layer forms, the radial dependence will be

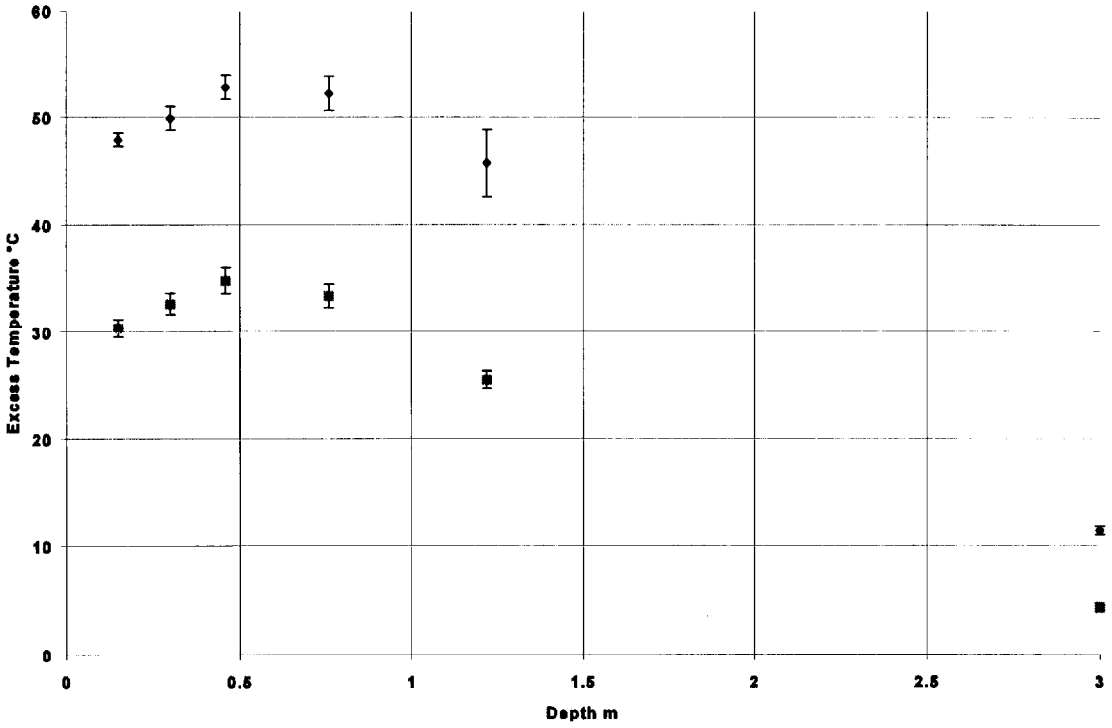

Figure 7 Excess temperature as a function of depth for the 7.7 MW JP-5 pan fire without draft curtain at Barbers Point. The squares represent a measurement time of 100 s while the diamonds represent a measurement time of 400 s.

reduced to a minimum of 0.23 as the layer depth increases. The experimental value for this parameter is 0.23 ± 0.07. The value of β (maximum value equals 0.84) is based on the experimentally observed decrease in temperature difference between the plume centerline temperature and the ceiling jet temperature at r/H = 0.18 as the hot layer depth increases in time. Early in time, before a layer forms, the experimentally determined value of β is 0.67 ± .11 while once a layer forms, the value increases to 0.84 ± 0.04. This increase is caused by the decrease in the entrainment of cool gas into the ceiling jet due both to the presence of the hot layer and to the circulation of ceiling jet flow back into the plume by the draft curtains. The value of y_j was chosen to be 1.0 based on the observation that JP-5 plumes become optically thick at a diameter of approximately 1.0 m, thereby eliminating the energy loss by radiation once the layer has reached this thickness.

3.3 Ceiling Jet Temperature Variation With Depth Beneath The Ceiling

The temperature dependence as a function of vertical distance below the ceiling must be understood as the ceiling jet model developed for the computer model JET makes no accommodation for temperature changes with depth. Three experiments conducted at Keflavik plus the experiments conducted at Barbers Point had sufficient numbers of thermocouples in the vertical direction to resolve the vertical temperature structure near the ceiling. For the two experiments without draft curtains at Barbers Point (see figure 7 for the 7.7 MW fire without draft curtains at Barbers Point), the ceiling jet temperature reached a maximum value at roughly 0.5 m below the ceiling at which point a fairly rapid decline occurred, with the excess temperature being nearly zero at a depth of 3.1 m beneath the ceiling. From the data, the thickness of the ceiling jet for these experiments would range from 2.0 m to 3.0 m which is 14 percent to 21 percent times the fire to ceiling height distance. This is slightly thicker than the 5 percent to 12 percent of the fire to ceiling height suggested in [12].

The maximum temperature was reached at about 3 percent of the fire to ceiling height which is larger than the 1 percent value given in reference [12]. It should be noted that the difference in

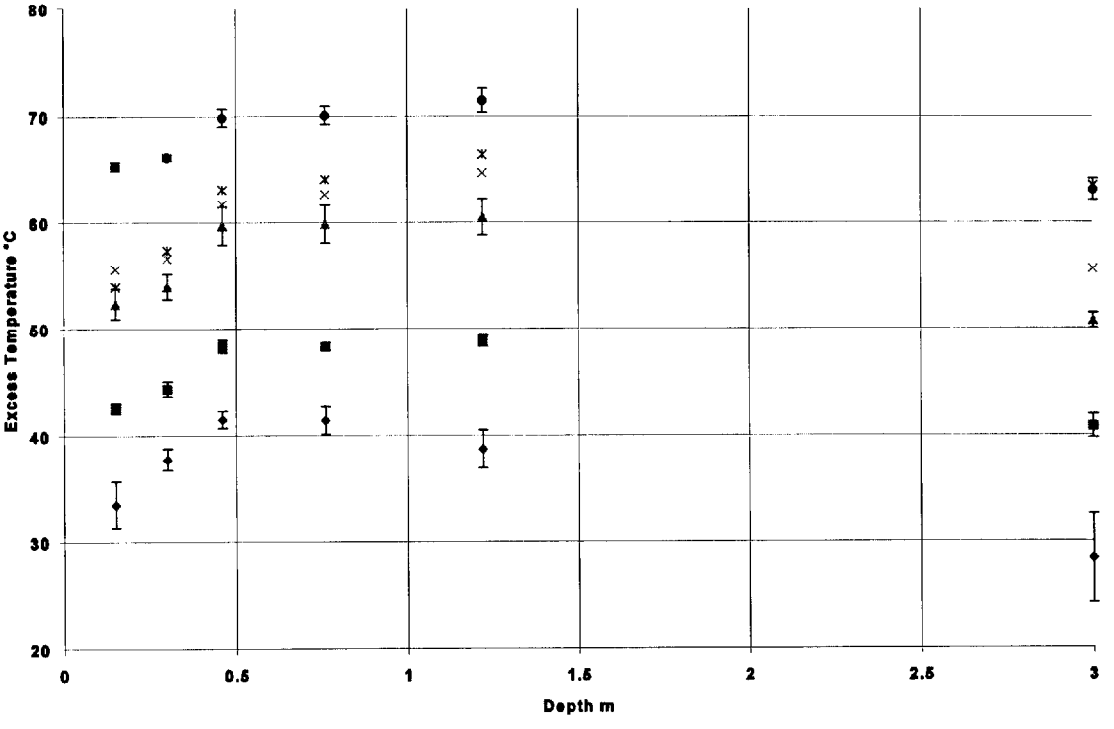

Figure 8 Excess temperature as a function of depth for the 7.7 MW JP-5 pan fire with draft curtain at Barbers Point. The data sets shown on the graph represent measurement times of 70 s, 100 s, 150 s, 200 s, 250 s, and 300 s from bottom to top respectively.

the position of the maximum temperature may be due to the presence of the ceiling I-beams of depth 0.25 m.

Once the layer forms, the temperature still requires roughly 0.5 m to reach its maximum value. It remains at this maximum value for a substantial distance beneath the ceiling. A good demonstration of this behavior is shown in figure 8 for the 7.7 MW fire with draft curtain at Barbers Point. Uncertainty intervals are not shown for two data sets in this figure in order to avoid cluttering the figure but the uncertainty intervals will be approximately the same as the ones shown in the figure. The thermocouple tree was located at 9.1 m east of fire center. At 70 s after the start of the fire, the maximum temperature of the ceiling jet is located at roughly 0.5 m beneath the ceiling. The temperature of the jet begins to decrease at about 1 m beneath the

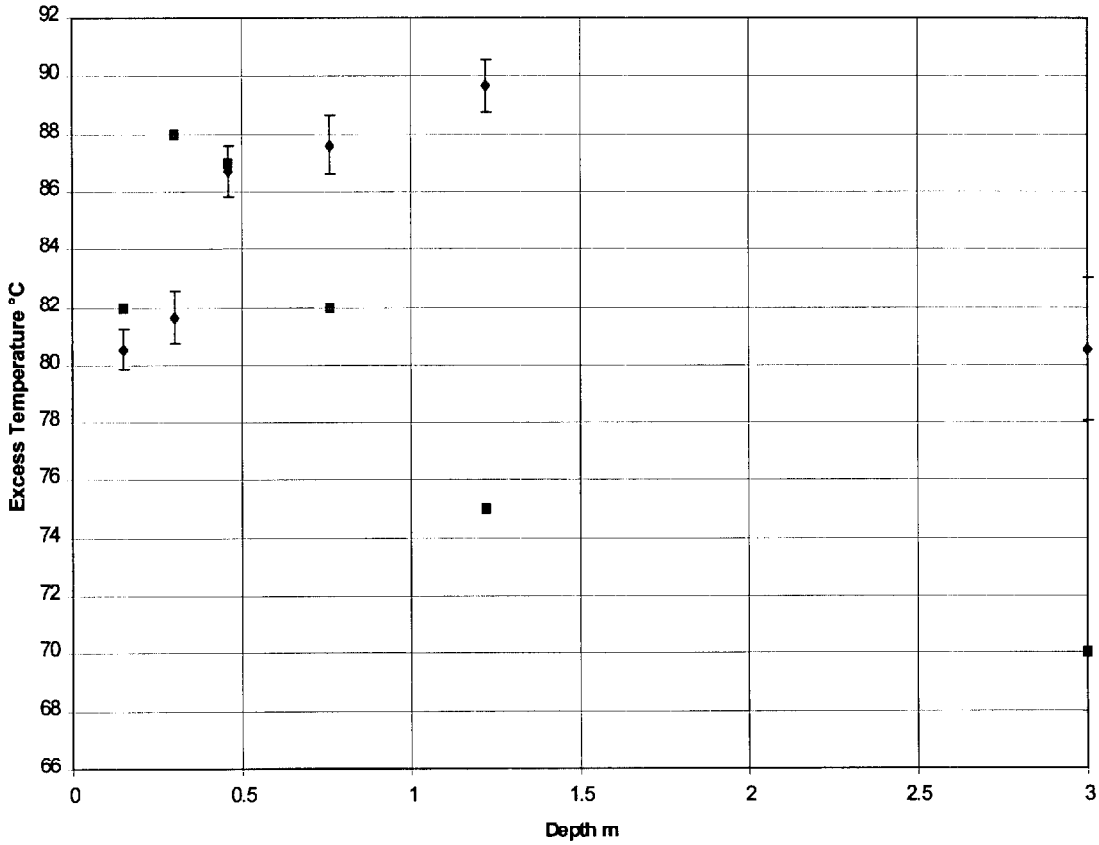

Figure 9 Comparison of the measured ceiling jet temperature profile at r = 9.1 m for the 7.7 MW JP-5 pan fire with a draft curtain. The diamonds represent the data at 200 s while the squares give the predictions of LAVENT. The excess temperature has a relative uncertainty of ± 7.5% but the shape of the temperature profile will not be affected by this uncertainty.

ceiling. At later times after a layer has formed, the temperature still rises rapidly for the first 0.5

m beneath the ceiling. It then remains either constant or rises slightly for the next 0.75 m. The depth at which the temperature begins to decline when a layer is present cannot be determined with the present data set.

A comparison of the temperature profile of the ceiling jet for the 7.7 MW fire with draft curtain at Barbers Point with the profile predicted by LAVENT is shown in figure 9. The ceiling jet model in LAVENT predicts the temperature maximum closer to the ceiling and yields a ceiling jet temperature profile which is substantially more narrow than observed. Comparing the predictions of LAVENT with the 7.7 MW fire without a draft curtain at Barbers Point (figure 10), the position of the maximum temperature point in the ceiling jet is again closer to the ceiling then measured but the shape of the ceiling jet profile is much closer to the measured profile.

While the temperatures predicted by LAVENT depend on the convective heat release rate, the shape of the profile is independent of the HRR. Therefore, while the temperatures calculated using LAVENT have a relative uncertainty of ±7.5%, the position of the temperature maximum will not change due to this uncertainty.

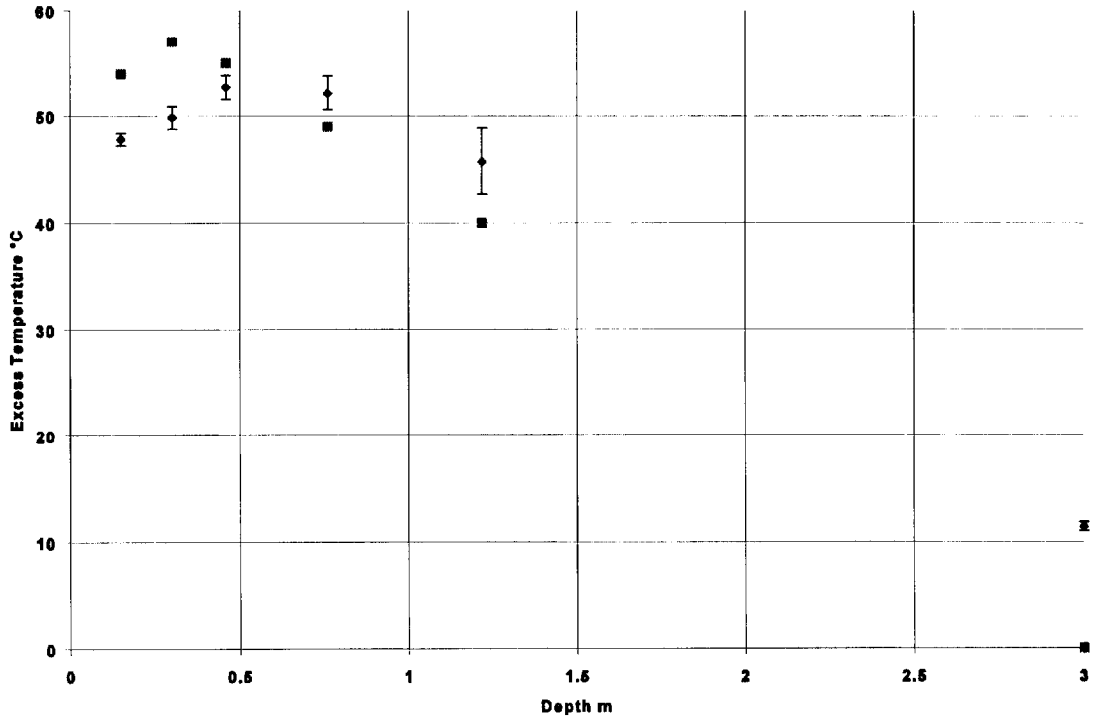

Figure 10 Comparison of the measured ceiling jet temperature profile at r = 9.1 m for the 7.7 MW JP-5 pan fire without a draft curtain. The diamonds represent the data at 400 s while the squares give the predictions of LAVENT.

The presence of the layer increases the depth over which the high temperatures persist near the ceiling. Since in both situations, with and without a layer, the high temperature region was at least 0.5 m in depth, the need to model the temperature fall off with depth beneath the ceiling is probably not important. The important issue is to establish the distance that the maximum temperature is reached beneath the ceiling as information relevant to optimizing the response of thermal detectors and sprinklers.

The models FPEtool, LAVENT, and the proposed ceiling jet model (equations 9 - 13) are compared with the measured temperature 0.3 m beneath the ceiling at 200 s for the 14.6 MW test at Keflavik (figure 11). The proposed ceiling jet model used the layer temperature and height predictive capabilities of LAVENT which resulted in a new computational model designated JET. The models are compared with the averaged east-west data. Total temperature is used since FPEtool can only be run with an ambient temperature of 21 °C. The other two models used the measured ambient temperature of 14 °C. The radiative fraction used in the calculation for JET and FPEtool was taken from equation 9. LAVENT uses a fixed radiative fraction of 0.35 which is too high based on the earlier discussion of radiative fraction. Decreasing the radiative fraction for the LAVENT calculation would increase both the layer and ceiling jet temperature predictions.

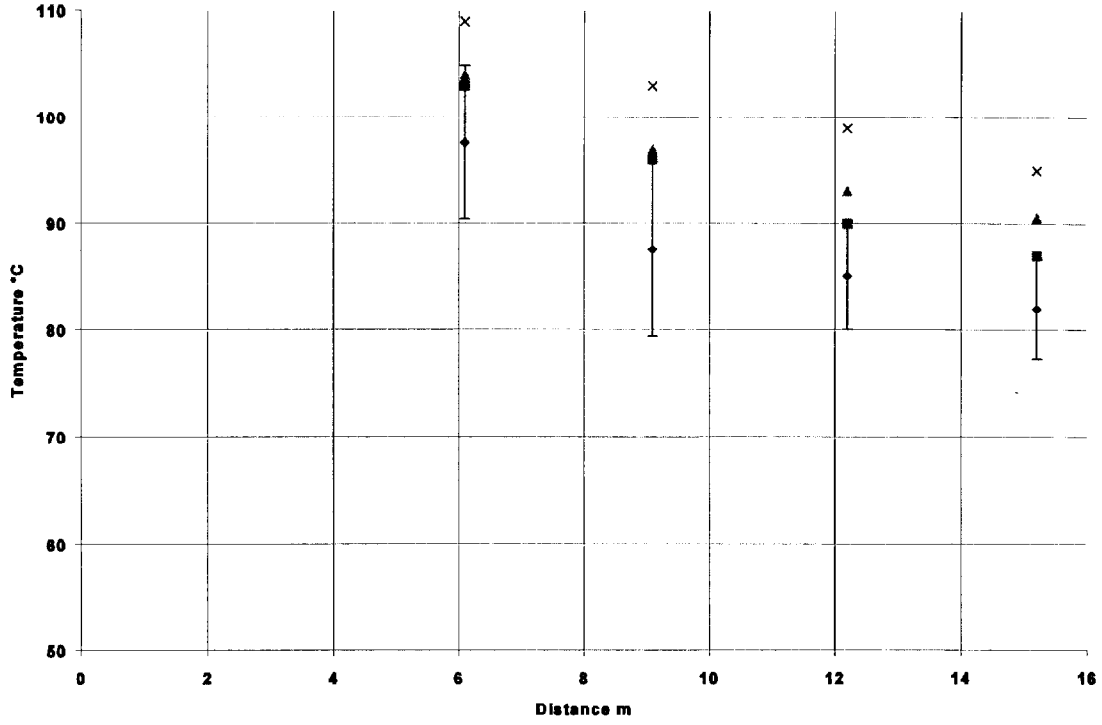

Figure 11 Comparison of ceiling jet temperature predictions of the models FPEtool (triangles), LAVENT (x), and JET (squares) with the measured values (diamonds) at 200 s for the 14.6 MW experiment at Keflavik. Uncertainty in the convective heat release rate will yield a relative uncertainty of ±6°C in the temperature predictions of the computer models but will not affect the radial temperature dependence.

All three models overpredict the measured ceiling jet temperature although JET and FPEtool provide predictions which lie inside the combined measurement uncertainty for the convective heat release rate and the experiment. All three models display a similar radial dependence with temperature which is similar to that measured in the experiment.

4. Detection Experiments

Heat detectors tested in the hangar experiments included analog addressable spot type detectors operating as fixed temperature heat detectors with an alarm threshold of 57.2 °C, a line type heat detector with a response time index (RTI) of 58 (m s)$^{1/2}$, and fusible elements with activation

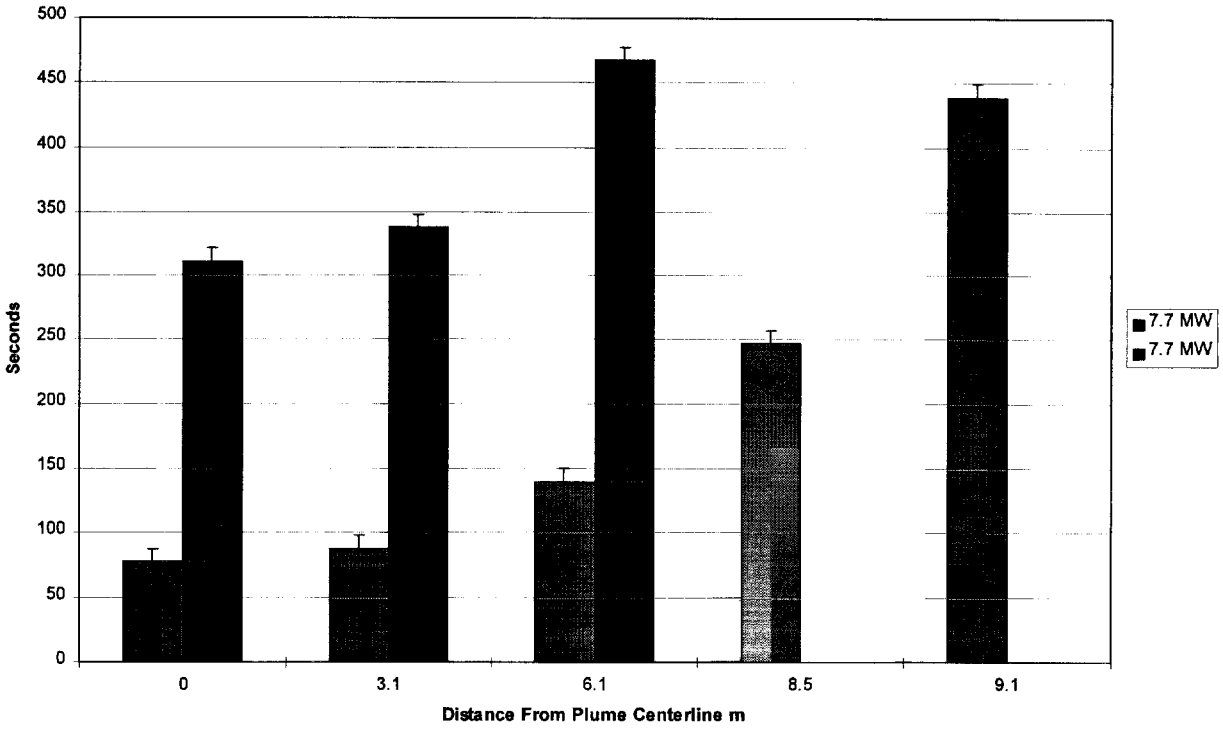

Figure 12 Earliest activation time for a 79 °C sprinkler bulb at each of the distances shown. The left or only bar gives the activation in the presence of a draft curtain while the right bar in pairs gives the activation when no draft curtain is present. Both tests were 2.5 m diameter JP - 5 pan fires in the 15 m hangar. The ±10 s uncertainty interval represents the uncertainty in the timing for the start of the experiment.

temperatures of 79 °C, 93 °C, 141 °C, and 182 °C. The fusible elements used were either quick response, 35 (m s)$^{1/2}$, or standard response, 95 (m s)$^{1/2}$ and 188 (m s)$^{1/2}$, links.

4.1 Fusible Elements

Threshold fire sizes for the activation of 79 °C links can be determined using the data presented in tables 1 and 4. For the 15 m hangar, a fire size of 5.6 MW was required to activate a 79 °C link located 3.1 m from plume center. While this experiment did not have a draft curtain in place, the activation time for the sprinkler was so late that a hot upper layer was beginning to develop in the entire hangar. For the 22 m hangar, a fire size of 7.9 MW was required to activate a 79 °C link located 3.1 m from plume center. In this case, a draft curtain was in place which caused a hot upper layer to form early in the experiment.

The presence of draft curtains produces a more uniform and higher temperature region within the draft curtain volume as discussed in the modeling section. This results in both the activation of fusible elements with smaller fire sizes and the earlier activation of fusible elements located away from plume center but within the draft curtains. These effects are readily seen in figure 12 for two 7.7 MW fires in the 15 m facility. The fire with draft curtains (3.7 m deep) caused 79 °C fusible elements to activate several minutes earlier than the fire without draft curtains for distances from fire center out to 6.1 m and produced activations at 8.5 m and 9.1 m which did not occur for the fire without draft curtains. It should be noted that the fusible links activated in the hangar fire without draft curtains at a time so late that an upper layer was beginning to develop in the entire hangar.

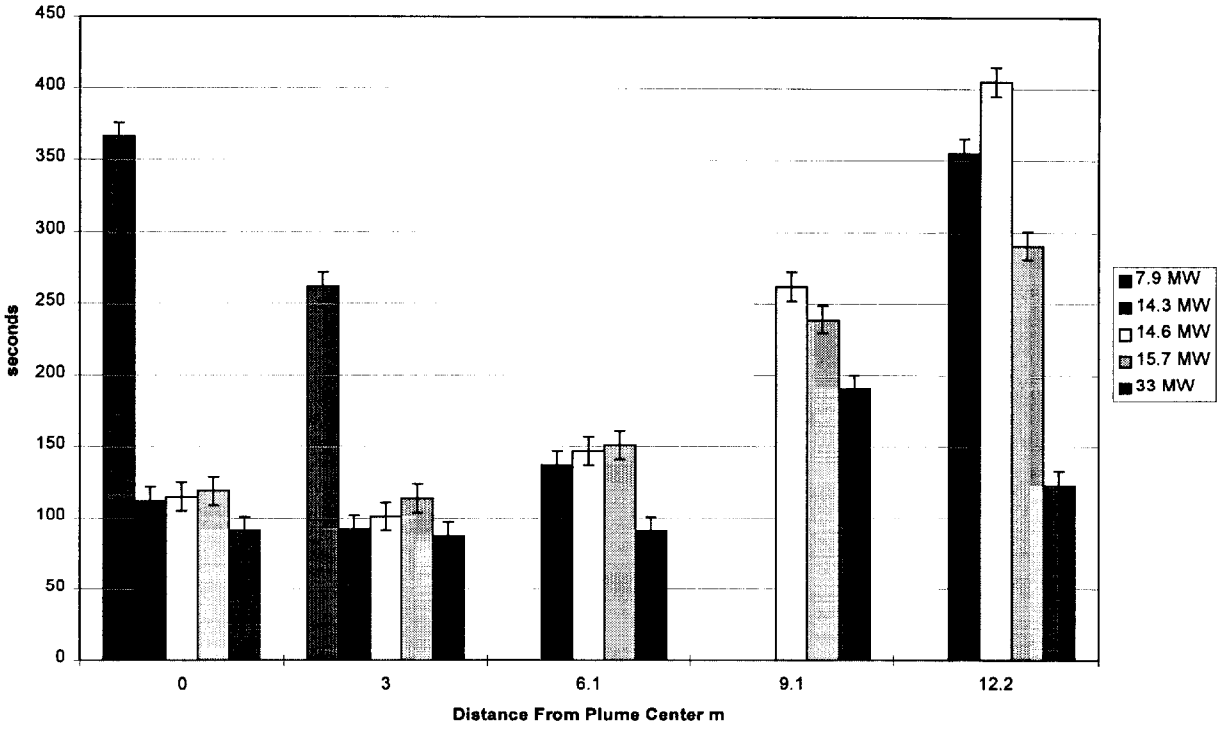

Figure 13 Earliest activation time of 79 °C sprinkler bulbs in the 22 m hangar as a function of distance and fire size. The fires are identified by total heat release rate. Uncertainties in these heat release rates are given in table 4. The ±10 s uncertainty interval represents the uncertainty in the timing for the start of the experiment.

All the experiments conducted in the 22 m hangar had draft curtains present in the direction perpendicular to the curved ceiling. Figure 13 gives the first activation time at each radial position in the direction of the curved ceiling for 79 °C fusible links. For the threshold fire at 7.9 MW, fusible links activated only in the plume region ($r/H < 0.2$). Fires of size 14 MW to 16 MW produced activations requiring less than 200 s for distances up to 6.1 m from plume center while a 33 MW fire activated all the elements out to 12.2 m in less than 200 s. Activation times for fires 14 MW or larger were within 60 s of each other for sprinklers at distances out to 6.1 m. The impact of the curved ceiling on detector activation was unimportant for distances up to 6.1 m from plume center for these fire sizes. The similar activation times measured out to 6.1 m resulted from the formation of a hot upper layer which produced a more uniform temperature environment as discussed in the modeling section.

4.2 Heat Detectors

The heat detector response to the fires in the two facilities were similar to the sprinkler element responses. Differences between the two types of detectors were primarily due to the activation temperatures of the heat detectors being lower at 57 °C and the lack of thermal lag typical of sprinkler elements (the heat detectors use a non-metallic thermistor). The impact of the presence of the draft curtain is easily demonstrated in figure 14. All heat detectors in the draft curtained area activated at essentially the same time while for the fire with no draft curtains, substantial delays occurred once the distance from plume centerline reached 8.5 m.

The impact of threshold fires on detector spacing is demonstrated in figure 15. Here, a 2.8 MW fire produces activation out to 9.1 m but activation times increase substantially with distance. A 7.7 MW fire produces nearly identical activation times across the draft curtained area. Hence, in a draft curtained area, if detection is designed for threshold fires, detector spacing should be reduced with the spacing set at the expected plume width. For non threshold designs, detector spacing can be increased substantially with the use of draft curtains.

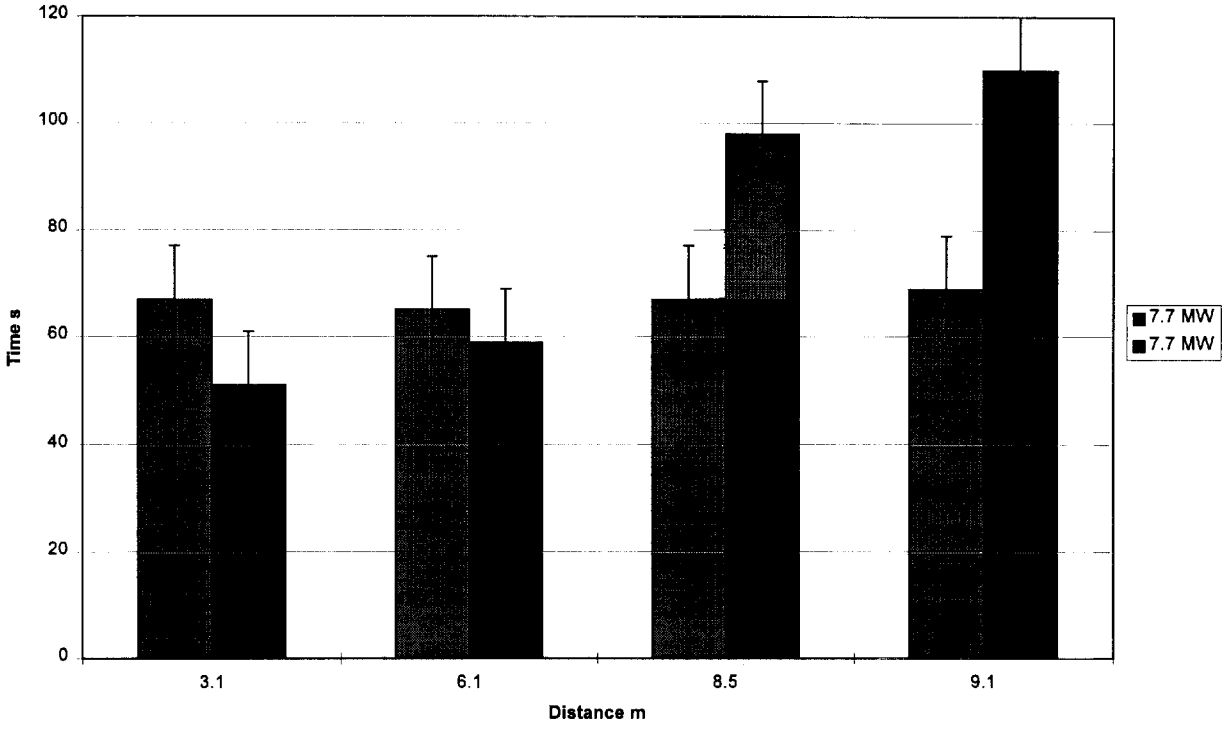

Figure 14 Earliest activation time for 57 °C heat detectors as a function of distance for the 2.5 m diameter JP - 5 pan fires with and without a draft curtain in the 15 m hangar. The draft curtain tests are represented by the left bar at each position. The ±10 s uncertainty interval represents the uncertainty in the timing for the start of the experiment.

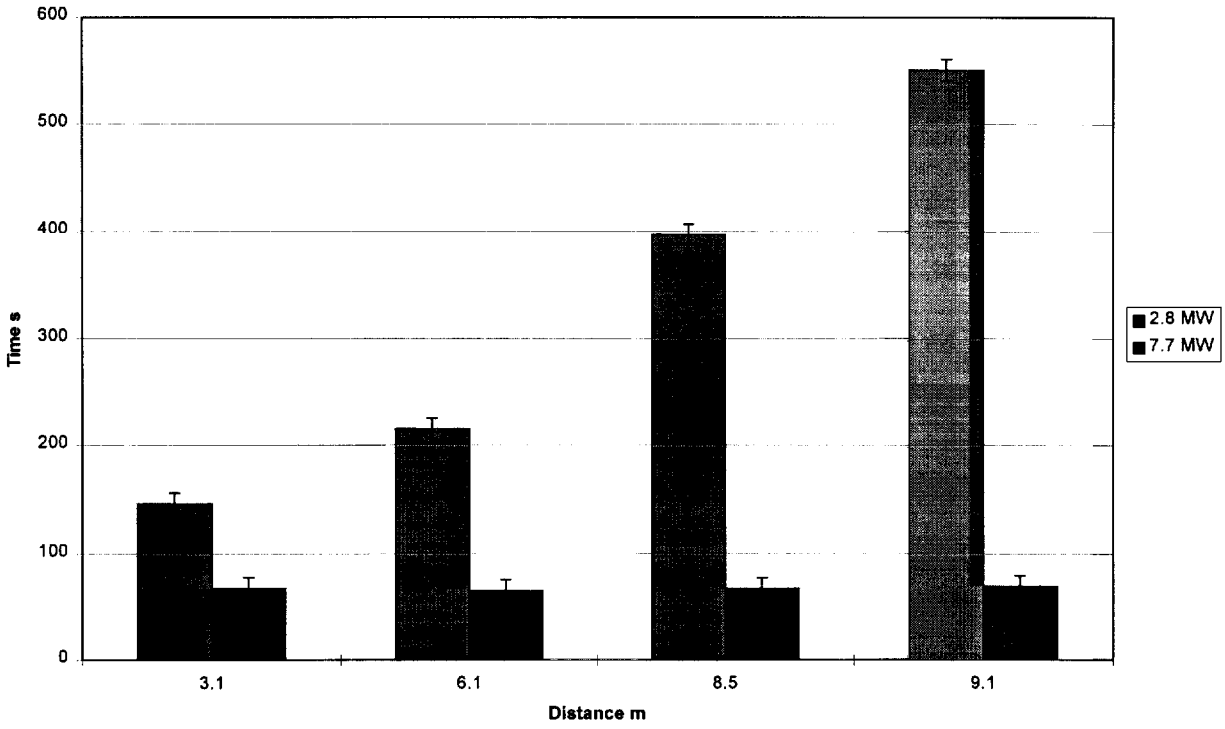

Figure 15 Earliest activation times as a function of distance for 57 °C heat detectors in the 15 m Hangar for two tests which have draft curtains. The ±10 s uncertainty interval represents the uncertainty in the timing for the start of the experiment.

For the tests in the 22 m facility, a 4.9 MW fire was just able to activate one heat detector at 6.1 m as shown in figure 16 which would represent a fire at threshold. As the fire size was increased to 7.9 MW, activation times varied substantially with distance from plume center. For fires larger than 14 MW, activation times showed a reduced dependence on distance from plume center.

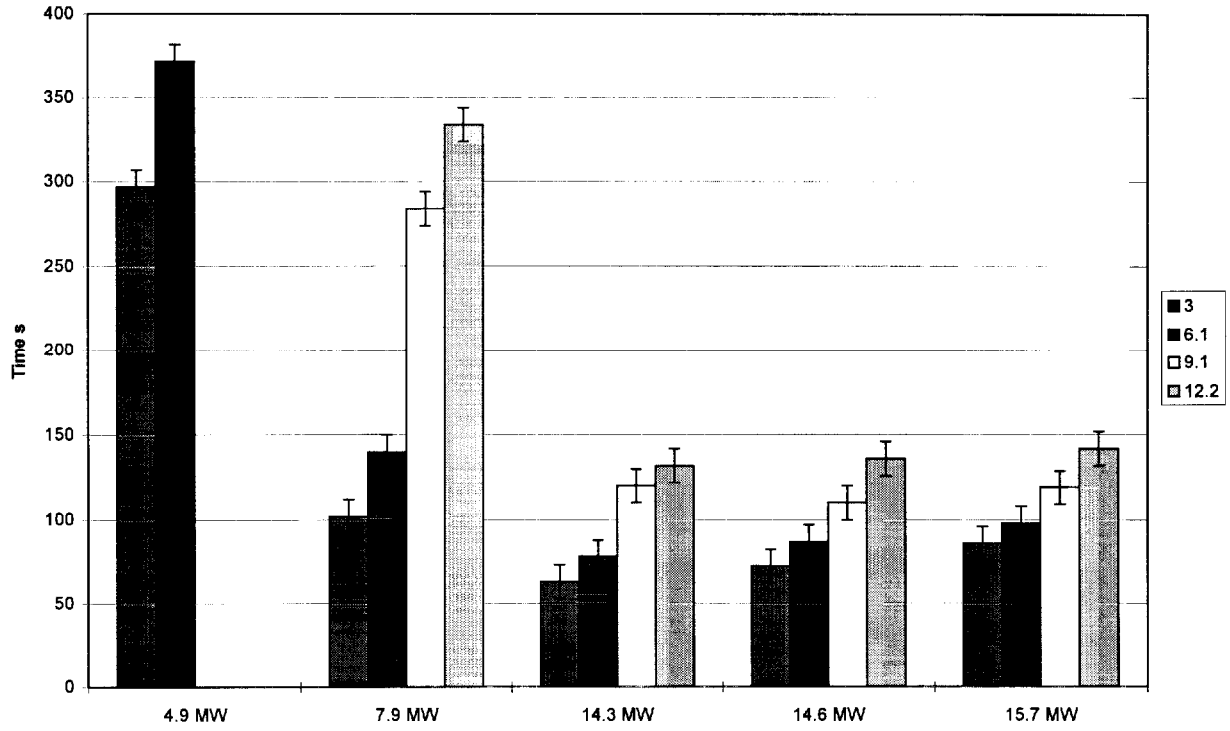

Figure 16 Earliest activation times as a function of distance for 57 °C heat detectors in the 22 m hangar. Distances from fire center are given in the side box in meters. The ±10 s uncertainty interval represents the uncertainty in the timing for the start of the experiment.

4.3 Smoke Detectors

The activation of photoelectric smoke detectors in the 15 m and 22 m experiments were typically quicker and were sensitive to smaller fire sizes than the heat detectors (see tables 1 and 3). For the photoelectric smoke detectors, no activation was observed for the 100 kW fire size. Smoke detectors activated between 23 s and 61 s for fire sizes of 500 kW and larger. The activation times for these larger fires will not correlate with fire size since the smoke detectors were

activating during the growing phase of the fire. The presence of draft curtains did not affect activation times. The reason for this is that the smoke detectors were located in the ceiling jet and would only be marginally affected by a developing layer. Based on the 15 m experiments, spacing for the ceiling mounted smoke detectors could be as large as 12 m and produce substantially the same activation time for the JP-5 fires. Similar results were observed for wood cribs fires where a 600 kW fire produced activation of smoke detectors to 6 m on either side of plume center without substantial loss in detection time.

The response of projected beam detectors to the fires were as expected (see tables 1 and 3). Activation occurred in less than a minute for beams located near the ceiling which sampled the ceiling jet. For beams located below the ceiling jet and outside of the plume region, activation occurred at acceptable times only when the beam sampled the smokey layer created by the draft curtains. These detectors were able to detect the 100 kW test fires in less than two minutes after the start of the fire. One problem that was observed with these detectors was that many times trouble signals rather than alarms were registered due to the very dense smoke produced by the JP-5 fires which completely obscured the beam. The alarm window was reduced from 30 s to 5 s for the 22 m experiments which eliminated the trouble signals for all but one of the open door tests. Trouble signals were not a problem for the wood pallet fires due to the less dense smoke produced by this type of fire.

4.4 Impact of Beams on Detection

The impact of the presence of beams could be analyzed with the 15 m data since the roof was supported by 0.25 m I beams which ran in the N-S direction and would therefore impede the flow of smoke in the E-W direction. Table 6 gives the activation times in the north, south, east, and west directions for spot smoke detectors operating at a radial distance of 6.1 m from plume center for the two 500 kW fires which were the smallest fires to activate the smoke detectors. The smoke detectors activate at roughly the same time in all directions except for the east direction in test 2 which activated at a substantially earlier time. The reason for this activation is that the plume leaned to the east early in this test which would favor the activation of smoke detectors in this direction. Ceiling beams of this size seem to have little impact on smoke detector activation for high ceiling fires probably due to the increased thickness of the ceiling jet with height. The beams in this study supported a corrugated roof and the seal between the beams and the roof was not perfect.

Table 6 Photoelectric smoke detector response times (s). The label "nd" indicates that no detector was present at that location.

Location	3.0 m	6.1 m	8.5 m	9.1 m
Test 2 - 500 kW with draft curtain				
North	27 ± 10	44 ± 10	40 ± 10	nd
East	23 ± 10	35 ± 10	nd	73 ± 10
South	32 ± 10	53 ± 10	48 ± 10	nd
West	31 ± 10	60 ± 10	nd	81 ± 10
Test 12 - 500 kW without draft curtain				
North	58 ± 10	53 ± 10	58 ± 10	nd
East	61 ± 10	49 ± 10	nd	153 ± 10
South	41 ± 10	49 ± 10	58 ± 10	nd
West	40 ± 10	57 ± 10	nd	115 ± 10

Table 7 gives the activation times in the north, south, east and west directions for the 57 °C spot heat detectors for all distances inside the draft curtain. If the 0.25 m I beams impacted the flow of hot smoke across the ceiling, the detectors in the E-W direction should activate at later times than the detectors in the N-S direction. As can be seen from the table, activation times did not appear to be dependent on direction which again suggests that these detectors were not impacted by the presence of the beams.

4.5 Impact of Wind

The impact of wind on the activation of detectors can be analyzed by comparing the activation history of the open door tests (#13 at Barbers Point and #16 and #19 at Keflavik, see tables 1 and 4) with the corresponding closed door tests (#7 at Barbers Point and #14 at Keflavik). In both closed door tests, 79 °C sprinklers activated. For the open door tests, none of the 79 °C sprinklers activated. The temperatures measured at the ceiling for the open door tests were substantially less than for the closed door tests. With two doors open in the 15 m hangar, the temperature measured at the ceiling reached only 58 °C ± 2 °C compared with 90 °C ± 2 °C for a similar fire size with both doors closed. For the 22 m hangar, with two doors open, the ceiling temperature reached 66 °C ± 2 °C, with one door open 77 °C ± 2 °C while with both doors

closed it reached 93 °C ± 2 °C. Wind speeds were measured to range from 14 km/h to 32 km/h 10.4 m north of fire center and 3 m above the floor in the 15 m hangar. In the 22 m hangar, the two door open test had wind speeds which ranged from 4 km/h to 7 km/h, 7 m south of fire center and 0.8 m above the floor while the one door open test had wind speeds which ranged from 2 km/h to 6 km/h, 5.7 m south of fire center and 0.8 m above the floor. Wind speed measurements have an uncertainty of ±1 km/h.

From a smoke obscuration standpoint, the one door open experiment produced substantially more mixing of smoke into the lower layer than the two door open experiments. In the one door open experiment, the smoke near the ceiling was observed to flow to the back of the hangar, deflect downward and flow back toward the fire near the floor. By 240 s into the fire, the floor area was very smokey and by 330 s, all personnel without breathing apparatus had to be evacuated from the building. In both two door open experiments, the smoke mixing into the lower layer did not become severe enough to require an evacuation.

Smoke detector activation times were unaffected by the wind for all three open door tests. The smoke detectors downwind from the fire typically were the first detectors to activate with the upwind detector activating at later times.

Table 7 57 °C heat detector response times (s) in 15 m high hangar. The entry "nd" indicates that no detector was installed at that position.

Location	3.0 m	6.1 m	8.5 m	9.1 m
Test 5 - 6.8 MW with draft curtain				
North	92 ± 10	96 ± 10	154 ± 10	nd
East	71 ± 10	88 ± 10	nd	121 ± 10
South	80 ± 10	92 ± 10	113 ± 10	nd
West	71 ± 10	100 ± 10	nd	175 ± 10
Test 6b - 7.7 MW with draft curtain				
North	65 ± 10	65 ± 10	69 ± 10	nd
East	69 ± 10	27 ± 10	nd	69 ± 10
South	19 ± 10	65 ± 10	65 ± 10	nd
West	85 ± 10	69 ± 10	nd	32 ± 10
Test 7 - 5.6 MW without draft curtain				
North	188 ± 10	92 ± 10	200 ± 10	nd
East	75 ± 10	138 ± 10	nd	274 ± 10
South	84 ± 10	101 ± 10	138 ± 10	nd
West	63 ± 10	113 ± 10	nd	167 ± 10
Test 8 - 7.7 MW without draft curtain				
North	59 ± 10	59 ± 10	105 ± 10	nd
East	51 ± 10	59 ± 10	nd	96 ± 10
South	51 ± 10	67 ± 10	92 ± 10	nd
West	51 ± 10	75 ± 10	nd	125 ± 10

5. Prediction Based Design

Planning for the detection of fire in high bay spaces is complicated by the substantial dilution in smoke concentration and reduction in temperature of the fire plume due to the entrainment of cool ambient air. The computer models discussed in this paper may be used to estimate plume centerline temperature and ceiling jet temperature. Knowledge of these temperatures coupled with experimental verification of detector activation for the hangar experiments provide a framework for detector analysis in these spaces.

The NASA inventory contains a broad spectrum of building types and uses. The following example is designed to provide a framework for NASA engineers to apply to specific facilities. It will be assumed that the facility under consideration is not a clean room and could be protected by ceiling mounted detectors. The fire will be assumed to be located away from structure walls with no substantial blockages located between the fire and the ceiling. Temperature stratification as a function of height is assumed to be negligible. The impact of wind on detector operation will be ignored.

A. The most important design parameters for ceiling mounted heat detectors are the temperature at plume center and the ceiling jet temperature at half the projected detector spacing. Estimates of these temperatures can be made using the following procedure.

   1. Identify the minimum heat release rate desired to detect and the type of fuel.

   2. Determine the radiative fraction of the fuel. If the radiative fraction of the fuel is not known, a radiative fraction of 0.4 is recommended as this value will approximate a conservative scenario (see for example radiative fractions for various size hydrocarbon pool fires[18]). The radiative fraction will depend not only on fuel type but also on fire size. It is best to use a variable radiative fraction if the correlation between radiative fraction and fire size is known (see reference 14 for guidance).

   3. Estimate the expected minimum ambient temperature for the space. This temperature will be used as the ambient temperature in the following calculations.

   4. If draft curtains are present, the computer zone fire model JET can be used to estimate the plume centerline temperature and ceiling jet temperature at half the desired spacing of the detector as a function of layer depth.

   5. If draft curtains are not present, the "no layer" option of the computer zone fire model JET or Heskestad's plume correlation and Alpert's ceiling jet correlation can be used to estimate these temperatures.

B. The calculated temperatures at plume center and at the half spacing point represent the maximum theoretical temperatures for heat detector response at the minimum heat release

rate. Uncertainties in the calculations and response temperature of the hardware should be considered in selecting heat detectors designed to respond at lower temperatures than the maximum theoretical value calculated. Sources of uncertainty not included in the calculation are plume motion, fire puffing, the presence of forced air flow, and conductive heat losses by the detector. While the impact of plume motion is important, for an array of detectors, plume motion may delay the activation of some detectors while decreasing the time for activation of other detectors.

The design activation temperature may be estimated by decreasing the calculated maximum theoretical temperature by the manufacturer's uncertainty for the detector. The design activation temperature would represent the temperature rating that a heat detector or fusible element should have in order to activate for the minimum fire size. For example, suppose that for a given target fire size, calculations show that the maximum theoretical temperature at half the detector spacing is 65 °C. If the manufacturing uncertainty for the detector of choice is ±5 °C, then the design activation temperature for the detectors would be 60 °C. This example neglects the effects of forced air flow and fire puffing. It is assumed that the manufacturer's uncertainty includes the effects of heat conduction. For regions where forced air flow may be a problem, some guidance can be found in reference 17.

C. The fire size for the activation of smoke detectors may be estimated in the following manner. Either the "no layer" option of the zone fire model JET or Heskestad's plume correlation and Alpert's ceiling jet correlation may be used to calculate the excess temperature at the ceiling for a given heat release rate. Analysis has shown [17] that a 5°C excess temperature will activate smoke detectors with sensitivity of 8.2 %/m for typical hydrocarbon fires. This target temperature is valid only for hydrocarbon fires and should not be used for other types of fires. If the calculated excess temperature is less than 5 °C for a given fire size, the smoke detector would not be expected to activate at that location.

D. In the case of projected beam detectors, if the fuel type produces dense smoke, a trouble alarm rather than a fire alarm may be sent by the detector. In these instances, the alarm window can be modified to reduce the sampling time for determination of a trouble signal. In this study, a 5 second alarm window prevented trouble signals for all but one open door test for the 22 m hangar.

The analysis of the 15 m and 22 m high experiments indicates that draft curtains improved the activation times of ceiling mounted sprinklers and heat detectors and reduced the size of the threshold fires required to activate these systems. If fusible elements are used to control sprinklers, experiments [1] indicate that quick response heads produced substantially quicker activations than standard response heads at these heights

6. Computer Modeling

In order to gain some additional insight into the role that computer modeling can play, the 15 m detector results have been examined with the computer model JET to confirm its predictive capability. For smoke detection, the 15 m experiments showed that smoke detectors would activate for 500 kW fires but not for 100 kW fires. The predictions of the computer model JET for the 15 m facility agreed that the 5 °C excess temperature threshold would not be reached with a 100 kW fire. A 200 kW fire is predicted by JET to activate smoke detectors out to 9.1 m from fire center and would therefore represent the predicted threshold fire size for smoke detectors at this ceiling height.

For the 57 °C heat detectors, detectors activated out to a radial distance of 9.1 m from fire center for a fire size of 2.8 MW in the presence of draft curtains. A 1.1 MW fire size was not large enough to activate the detectors. JET predicted that heat detectors would activate for fire sizes as small as 2.0 MW out to 6.1 m as long as draft curtains were present but that a 2.8 MW fire would not activate heat detectors if no draft curtains were present.

For the 79 °C sprinklers, a sprinkler located at 3.1 m activated late in time for the 5.6 MW test with no draft curtain. The prediction of JET was that a 5.6 MW fire would not activate a 79 °C sprinkler link unless a draft curtain was present but in the presence of a draft curtain, activation would occur out to 9.1 m. The observed long delay in activation of the sprinkler head for this test (see Table 1) probably was the result of the entire hangar beginning to build up an upper layer and hence simulate the presence of a draft curtain. This long delay would support the predictions of JET.

Since the temperature excess at the ceiling scales as $Q^{2/3}/H^{5/3}$, extrapolating these results to other ceiling heights is straight forward. For 9 m ceilings, the threshold fire sizes are reduced to 0.28 times the 15 m sizes. For 18 m ceilings, the threshold fire sizes are increased by 1.6 times the 15 m sizes. For detectors placed at other radial distances from the fire center, JET could be used to refine the appropriate threshold fire sizes for detector activation.

The computer model JET is presently undergoing additional testing using experiments with lower ceiling heights and different fuel types. Once this testing is complete, the model can be made available for general distribution.

7. Summary

The following observations can be made concerning the application of detectors and use of fire modeling in spaces with ceiling heights between 9.1 m and 18 m.

1. The problems using zone fire models reported in reference [1] have been investigated and new algorithms developed. The new algorithms provide temperature predictions at plume center and in the ceiling jet which are in agreement with the experimental results reported in this paper. The new algorithms are available in the zone fire model JET and are being

incorporated into the zone model CFAST.

2. The presence of draft curtains decreased the response time of heat detectors and sprinklers tested in these experiments. Detectors respond to smaller fires when draft curtains are present. The impact of the fire plume located at the intersection of two adjacent curtained areas was not studied in these experiments as the test fires were always located in the geometric center of the curtained space.

3. When located near the center of the curtained area, the presence of draft curtains effectively contained the fire plume and resulted in a relatively flat temperature distribution within the curtained area with no significant temperature increase in adjacent areas. Thus it should be possible for automatic fire sprinkler systems to activate and control or extinguish fires under a single curtained area without the need for deluge systems that apply agent over the entire hangar area.

4. For ceiling heights of 9 m, NFPA 72 recommends that the linear spacing of heat detectors will be reduced to 3.0 m. The experiments in this study demonstrated that in a draft curtained area, if detection is designed for threshold fires, detector spacing should be set at the expected plume width. For non threshold designs, detector spacing may be increased to as much as 12 m at a ceiling height of 15 m without affecting activation times.

5. Ceiling beams of depth 0.25 m had no effect on the activation of smoke and heat detectors in this study.

6. For the experiments reported in this paper, 0.25 m beams caused the maximum ceiling jet temperature to occur at approximately 0.5 m beneath the ceiling. The expected smooth ceiling depth for maximum ceiling jet temperature for these experiments is approximately 0.2 m. The difference in depth is approximately equal to the beam width.

7. Beam type smoke detectors proved to be the most sensitive to small fires of the smoke detector types tested but also registered a number of trouble signals in response to the dense smoke produced by JP-5 pool fires.

8. In the presence of wind blowing through open doors, heat detectors and sprinklers would not be expected to activate at the same fire sizes predicted to activate these detectors when no wind is present. Smoke detector activation will be affected by the wind in that only the downwind detectors will activate for small fire sizes.

8. References

1. Gott, J.E., Lowe, D. L., Notarianni, K. A., and Davis W., "Analysis of High Bay Hangar Facilities for Detector Sensitivity and Placement," National Institute of Standards and Technology, *NIST Technical Note 1423*, Gaithersburg, MD (1997) pp. 1- 315.

2. Davis, W. D., Notarianni, K. A., and McGrattan, K. B., "Comparison of Fire Model Predictions with Experiments Conducted in a Hangar with a 15 Meter Ceiling," National Institute of Standards and Technology, *NISTIR 5927*, Gaithersburg, MD (1996) pp. 1-59.

3. Davis, W. D., Notarianni, K. A., and Tapper, P. Z., "An Algorithm for Calculating the Plume Centerline Temperature and Ceiling Jet Temperature in the Presence of a Hot Upper Layer.", *NISTIR 6178*, Gaithersburg, MD (1998) pp. 1-23.

4. NFPA 72, " National Fire Alarm Code," *National Fire Protections Association*, Quincy, MA (1993)

5. "Beam Smoke Detection Systems Installation Instructions," Detection Systems Inc., Fairport, NY (1994).

6. Heskestad, G., "Engineering Relations for Fire Plumes," *Fire Safety Journal*, Vol. 7, No. 1 (1984) pp. 25-32.

7. Cooper, L. Y., "Fire-Plume-Generated Ceiling Jet Characteristics and Convective Heat Transfer to Ceiling and Wall Surfaces in a Two-Layer Zone-Type Fire Environment," National Institute of Standards and Technology, *NISTIR 4705*, Gaithersburg, MD (1991).

8. Evans, D. D., "Calculating Sprinkler Actuation Time in Compartments," *F. Safety J.*, 9, 1985, pp. 147-155.

9. Peacock, R. D., Forney, G. P., Reneke, P., Portier, R., and Jones, W. W., "CFAST, the Consolidated Model of Fire Growth and Smoke Transport," *National Institute of Standards and Technology*, NIST TN 1299, 1993, pp. 1-235.

10. Deal, S., "Technical Reference Guide for FPEtool, Version 3.2," *National Institute of Standards and Technology,* NISTIR 5486-1, 1995, pp. 1-127.

11. Davis, W. D., and Cooper, L. Y., "Estimating the Environment and the Response of Sprinkler Links in Compartment Fires with Draft Curtains and Fusible Link-Actuated Ceiling Vents - Part II: User Guide for the Computer Code LAVENT," *National Institute of Standards and Technology*, NISTIR 89-4122, 1989, pp. 1-36.

12. Alpert, R. L., "Calculation of Response Time of Ceiling-Mounted Fire Detectors," *Fire Technology,* 8, 1972, pp. 181-195.

13. Heskestad, G., and Delichatsios, M. A., "The Initial Convective Flow in Fire," *17th International Symposium on Combustion, Combustion Institute, Pittsburgh* , 1978, pp. 1113-1123.

14. Yang, J. C., Hamins, A., and Kashiwagi, T., "Estimate of the Effect of Scale on Radiative Heat Loss Fraction and Combustion Efficiency," *Combustion Science and Technology,* 96, 1994, pp. 183-188.

15. Evans, D. D. And Stroup, D. W., "Methods to Calculate the Response Time of Heat and Smoke Detectors Installed Below Large Unobstructed Ceiling," *Fire Technology,* 22, No. 1 (1986) p. 54-65.

16. Zukowski, E. E., and Kubota, T., "An Experimental Investigation of the Heat Transfer from a Buoyant Gas Plume to a Horizontal Ceiling, Part II. Effects of Ceiling Layer," *National Institute of Standards and Technology,* NBS-GCR-77-98, 1975, pp. 1-73.

17. Davis, W. D., and Notarianni, K. A.,"NASA Fire Detector Study," *National Institute of Standards and Technology,* NIST 5798, 1996, pp. 1-33.

18. Mudan, K. S. and Croce, P. A., "Fire Hazard Calculations for Large Open Hydrocarbon Fires", *SFPE Handbook for fire Protection Engineering 2st ed.*, National Fire Protection Association, Quincy, Mass., 1995, p. 3-206

NIST-114
(REV. 6-93)
ADMAN 4.09

U.S. DEPARTMENT OF COMMERCE
NATIONAL INSTITUTE OF STANDARDS AND TECHNOLOGY

MANUSCRIPT REVIEW AND APPROVAL

(ERB USE ONLY)

ERB CONTROL NUMBER | DIVISION

PUBLICATION REPORT NUMBER: NISTIR 6199 | CATEGORY CODE

INSTRUCTIONS: ATTACH ORIGINAL OF THIS FORM TO ONE (1) COPY OF MANUSCRIPT AND SEND TO THE SECRETARY, APPROPRIATE EDITORIAL REVIEW BOARD

PUBLICATION DATE: July 1998 | NUMBER PRINTED PAGES

TITLE AND SUBTITLE (CITE IN FULL)

Prediction Based Design of Fire Detection for Buildings with Ceiling Heights between 9 m and 18 m

CONTRACT OR GRANT NUMBER | TYPE OF REPORT AND/OR PERIOD COVERED

AUTHOR(S) (LAST NAME, FIRST INITIAL, SECOND INITIAL)

Davis, W. D. and Notarianni, K. A.

PERFORMING ORGANIZATION (CHECK (X) ONE BOX)

[x] NIST/GAITHERSBURG
[ ] NIST/BOULDER
[ ] JILA/BOULDER

LABORATORY AND DIVISION NAMES (FIRST NIST AUTHOR ONLY)

Building and Fire Research Laboratory, Fire Safety Engineering Division

SPONSORING ORGANIZATION NAME AND COMPLETE ADDRESS (STREET, CITY, STATE, ZIP)

National Aeronautics and Space Administration
NASA Headquarters

PROPOSED FOR NIST PUBLICATION

[ ]	JOURNAL OF RESEARCH (NIST JRES)	[ ]	MONOGRAPH (NIST MN)	[ ]	LETTER CIRCULAR
[ ]	J. PHYS. & CHEM. REF. DATA (JPCRD)	[ ]	NATL. STD. REF. DATA SERIES (NIST NSRDS)	[ ]	BUILDING SCIENCE SERIES
[ ]	HANDBOOK (NIST HB)	[ ]	FEDERAL INF. PROCESS. STDS. (NIST FIPS)	[ ]	PRODUCT STANDARDS
[ ]	SPECIAL PUBLICATION (NIST SP)	[ ]	LIST OF PUBLICATIONS (NIST LP)	[x]	OTHER
[ ]	TECHNICAL NOTE (NIST TN)	[x]	NIST INTERAGENCY/INTERNAL REPORT (NISTIR)		

PROPOSED FOR NON-NIST PUBLICATION (CITE FULLY) [x] U.S. [ ] FOREIGN

Journal of Fire Protection Engineering, One Liberty Square, Boston, MA.02109-4825

PUBLISHING MEDIUM

[x] PAPER [ ] CD-ROM
[ ] DISKETTE (SPECIFY)
[ ] OTHER (SPECIFY)

SUPPLEMENTARY NOTES

ABSTRACT (A 2000-CHARACTER OR LESS FACTUAL SUMMARY OF MOST SIGNIFICANT INFORMATION. IF DOCUMENT INCLUDES A SIGNIFICANT BIBLIOGRAPHY OR LITERATURE SURVEY, CITE IT HERE. SPELL OUT ACRONYMS ON FIRST REFERENCE.) (CONTINUE ON SEPARATE PAGE, IF NECESSARY.)

The analysis of hangar experiments (NIST TN 1423) with 15 m and 22 m ceiling heights has led to a better understanding of the evolution of a fire driven ceiling jet. This work has demonstrated the impact of the presence of a hot upper layer on the radial and vertical temperature profiles of the ceiling jet. The importance of using a fire size dependent radiative fraction is established which, when used in conjunction with models which account for the entrainment of upper layer gas into the plume, provides better predictive capabilities for the plume centerline temperature. Plume and ceiling jet algorithms, which model the observations, have been developed and embedded in a new zone fire model.

The analysis of detector response using these experiments has resulted in the ability to establish threshold fire sizes for using smoke and heat detectors. It has also led to the recommendation of a lower temperature threshold to be used in computer models to determine smoke detector activation.

Guidelines for spacing of smoke and heat detectors are discussed. The importance of draft curtains at these heights is established, and the impact of the draft curtains on detector spacing is demonstrated. .

KEY WORDS (MAXIMUM OF 9; 28 CHARACTERS AND SPACES EACH; SEPARATE WITH SEMICOLONS; ALPHABETIC ORDER; CAPITALIZE ONLY PROPER NAMES)

ceiling jets; draft curtains; fire experiments; fire models; heat detectors; high bay; pool fires; smoke detectors; sprinkler response.

AVAILABILITY

[x] UNLIMITED [ ] FOR OFFICIAL DISTRIBUTION - DO NOT RELEASE TO NTIS
[ ] ORDER FROM SUPERINTENDENT OF DOCUMENTS, U.S. GPO, WASHINGTON, DC 20402
[X] ORDER FROM NTIS, SPRINGFIELD, VA 22161

NOTE TO AUTHOR(S): IF YOU DO NOT WISH THIS MANUSCRIPT ANNOUNCED BEFORE PUBLICATION, PLEASE CHECK HERE. [ ]

WORDPERFECT